Molecular Pharmacology Fast Forward. Published on July 10, 2019 as DOI: 10.1124/mol.119.116731
This article has not been copyedited and formatted. The final version may differ from this version.

Characterization and proteomic-transcriptomic investigation of monocarboxylate transporter 6 (Mct6) knockout mice: evidence of a potential role in glucose and lipid metabolism

Authors: Robert S. Jones [1], Chengjian Tu [1,2], Ming Zhang [2], Jun Qu [1,2], and Marilyn E. Morris [1, *]

[1] Department of Pharmaceutical Sciences, School of Pharmacy and Pharmaceutical Sciences, University at Buffalo, State University of New York, Buffalo, New York 14214, USA

[2] New York State Center of Excellence in Bioinformatics and Life Sciences, 701 Ellicott Street, Buffalo, NY, USA

Molecular Pharmacology Fast Forward. Published on July 10, 2019 as DOI: 10.1124/mol.119.116731
This article has not been copyedited and formatted. The final version may differ from this version.

Running title: Mct6 knockout mice and role in glucose and lipid metabolism

* Correspondence should be addressed to:

Marilyn E. Morris, PhD

Department of Pharmaceutical Sciences

University at Buffalo

State University of New York

352 Kapoor Hall

Buffalo, NY 14214

Ph: (716) 645-4839

memorris@buffalo.edu

This manuscript contains:

23 text pages

5 tables

7 figures

54 references

226 words in *Abstract*

444 words in *Introduction*

1536 words in *Discussion*

Nonstandard abbreviations: ALP: alkaline phosphatase, ALT: alanine aminotransferase, BUN: blood urea nitrogen, CRISPR/Cas9: clustered regularly interspaced short palindromic

Molecular Pharmacology Fast Forward. Published on July 10, 2019 as DOI: 10.1124/mol.119.116731
This article has not been copyedited and formatted. The final version may differ from this version.

repeats/crispr associated protein 9, FAM: fluorescein amidite, FC: fold-change, Gapdh: glyceraldehyde 3-phosphate dehydrogenase, GLU: glucose, gRNA: guide RNA, Hprt: hypoxanthine guanine phosphoribosyl transferase, Indel: insertion/deletion, KO: knockout, LC/MS: liquid chromatography/mass spectrometry, Mct: monocarboxylate transporter, NGS: next generation sequencing, NHEJ: nonhomologous end joining, PAM: protospacer adjacent motif, PCA: principal component analysis, qRT-PCR: quantitative real time-polymerase chain reaction, Slc16a5: solute carrier family 16 member 5, TP: total protein, TG: triglycerides, WT: wildtype

Molecular Pharmacology Fast Forward. Published on July 10, 2019 as DOI: 10.1124/mol.119.116731
This article has not been copyedited and formatted. The final version may differ from this version.

ABSTRACT

Monocarboxylate transporter 6 (MCT6, SLC16A5) is an orphan transporter with no known endogenous substrates or physiological role. Previous *in vitro* and *in vivo* experiments investigated MCT6 substrate/inhibitor specificity in *X. laevis* oocytes; however, these data remain limited. Transcriptomic changes in the livers of mice undergoing different dieting schemes have suggested that Mct6 plays a role in glucose and lipid metabolism. The objectives of this study were (1) to develop a novel knockout mouse model ($Mct6^{-/-}$) using CRISPR/Cas9 technology and (2) to characterize the KO animal model by examining physiological and biochemical parameters, and through global proteomic and liver transcriptomic profiling, to understand the physiological role of MCT6 *in vivo*. mRNA tissue analysis demonstrated knockout of Mct6, which showed greater than 90% knockdown of *Mct6* (*Slc16a5*) gene expression in all major tissues analyzed when normalized to $Mct6^{+/+}$ mice. Proteomic analyses identified greater than 4,000 unique proteins in kidney, liver, and colon tissues, among which 51, 38, and 241 proteins were significantly altered (respectively for each tissue) between $Mct6^{+/+}$ and $Mct6^{-/-}$ mice. Additionally, $Mct6^{-/-}$ mice demonstrated significant changes in 199 genes in the liver compared with $Mct6^{+/+}$ mice. *In silico* biological pathway analyses revealed significant changes in proteins and genes involved in glucose and lipid metabolism-associated pathways. This study is the first to provide evidence for an association of Mct6 in the regulation of glucose and lipid metabolism.

Molecular Pharmacology Fast Forward. Published on July 10, 2019 as DOI: 10.1124/mol.119.116731
This article has not been copyedited and formatted. The final version may differ from this version.

SIGNIFICANCE STATEMENT

This manuscript focuses on elucidating the innate biological role of an orphan transporter *in vivo*, which has not been investigated thus far. Using efficient and high throughput technologies, such as CRISPR/Cas9 gene editing, LC/MS/MS-based proteomic, and RNA-seq transcriptomic analyses, our laboratory provides the first existence and characterization of a Mct6 knockout mouse model. The evidence gathered in this manuscript, as well as other labs, support the importance of MCT6 in regulating a variety of glucose and lipid metabolic pathways, which may indicate its significance in metabolic diseases.

Molecular Pharmacology Fast Forward. Published on July 10, 2019 as DOI: 10.1124/mol.119.116731
This article has not been copyedited and formatted. The final version may differ from this version.

INTRODUCTION

The monocarboxylate transporter (MCT, *SLC16*) family of transporters consists of 14 isoforms, with MCTs 1-4 being extensively characterized (Jones and Morris, 2016). MCTs 1-4 transport essential monocarboxylate anions such as lactate and pyruvate, in a proton-dependent manner. Other MCT isoforms do not necessarily transport monocarboxylates, but are essential for the distribution of important endogenous compounds such as thyroid hormone to the brain (MCT8/10) (Abe et al., 2012; Dumitrescu et al., 2006; Friesema et al., 2003) and aromatic amino acids into cells (MCT10) (Halestrap and Meredith, 2004). Recent publications have identified potential clinical roles of MCT1/4 in cancer treatment, MCT8 in hypothyroidism-related Allan-Herndon-Dudley syndrome (Schwartz et al., 2005), MCT11 in diabetes (Rusu et al., 2017), and MCT12 in cataract development (Castorino et al., 2011; Dhayat et al., 2016). However, a substantial number of MCTs have yet to be "de-orphanized", and for these MCT transporters their physiological function and potential role in drug targeting or disease remains unknown.

Monocarboxylate transporter 6 (MCT6, SLC16A5), classified as an orphan transporter protein, is expressed in tissues involved in drug absorption and elimination (Gill et al., 2005; Kohyama et al., 2013) (note that Gil et. al refers to MCT6 as "MCT5" prior to changes in isoform nomenclature). Substantial changes in murine hepatic *Slc16a5* gene expression occurs in different dieting states, including fasting (Zhang et al., 2011b) and fenofibrate-supplemented (Lu et al., 2011) diets.

In the study evaluating the effects of fasting and fed diet on the murine liver transcriptome, *Slc16a5* was detected as the 6th most upregulated gene that was induced by 24-h fasting, with approximately a 5-fold increase in gene expression compared to expression after a normal diet (Zhang et al., 2011a). This was also the most up-regulated solute carrier protein within this analysis. Treatment of mice with fenofibrate resulted in a 3- to 6-fold upregulation of *Slc16a5* in murine liver (Lu et al., 2011). These data suggest that Mct6 may play a role in lipid metabolism due to its differential regulation following various diets.

In terms of substrate specificity, our lab and others have reported that MCT6 substrates include bumetanide, nateglinide, probenecid, and prostaglandin $F_{2\alpha}$ based on studies with human MCT6-transfected

Molecular Pharmacology Fast Forward. Published on July 10, 2019 as DOI: 10.1124/mol.119.116731
This article has not been copyedited and formatted. The final version may differ from this version.

X. laevis oocytes (Murakami et al., 2005). A series of dietary aglycone flavonoids were also shown to be inhibitors of human MCT6-mediated bumetanide transport in *X. laevis* oocytes (Jones et al., 2017).

The goal of this study was to develop a novel CRISPR/Cas9 knockout mouse model of Mct6 deficiency and perform comparisons with WT Mct6$^{+/+}$ mice, including (1) physiological and biochemical parameters, (2) multi-tissue, global proteome profiling, and (3) a liver transcriptomic analysis. Pathway annotations were generated to better understand the physiological role of MCT6 *in vivo*.

Molecular Pharmacology Fast Forward. Published on July 10, 2019 as DOI: 10.1124/mol.119.116731
This article has not been copyedited and formatted. The final version may differ from this version.

MATERIALS AND METHODS

Ethics Statement.

Procedures involving mice were approved by and performed in accordance with the rules and recommendations of the Institutional Animal Care and Use Committee (IACUC) of the University at Buffalo.

Animals.

C56BL/6NCr and CD-1 mice were used for the *in vivo* studies (Charles River, Wilmington, MA). All mice were housed in cages with a 12 h light/12 h dark cycle. Animals were given free access to normal chow (Envigo 2018 Teklad global 18% protein extruded rodent diet) and water *ad libitum*. Blood was sampled via submandibular puncture. For tissue collection, mice were sacrificed via cardiac puncture and cervical dislocation.

Generation of CRISPR/Cas9 Mct6$^{-/-}$ mice.

The Mct6$^{-/-}$ mice were generated by Roswell Park Cancer Institute Gene Targeting and Transgenic Shared Resource (Buffalo, NY) and Washington State University in St. Louis Genome Engineering & iPSC Center (St. Louis, MO). Briefly, two short guide RNAs (gRNAs) (gRNA1 (5'-3'): AGCATCTTGGTCAAACATTT/**CGG**, gRNA2: CTGTGATCACTCCTGCGGTG/**AGG**; protospacer adjacent motif (PAM) sequences are underlined and in bold) were generated to target exon 2 in murine *Slc16a5* (Gene ID: 217316) (Fig. 1A). The gRNA sequences were verified in an off-target analysis screen prior to development and selected based on off-target profile and distance to the target site using the CRISPR design tool (http://crispr.mit.edu/). A mismatch detection assay for Cas9/gRNA activity was performed in a mouse neuroblastoma cell line (N2a) in order to verify targeted indel mutations via nonhomologous end joining (NHEJ) frequency, using CELI nuclease to detect mismatches (data not shown). Cas9 mRNA and gRNAs were injected into the cytoplasm of fertilized C57BL6/NCr embryos harvested the same day of microinjection. After injecting embryos, they were surgically implanted

Molecular Pharmacology Fast Forward. Published on July 10, 2019 as DOI: 10.1124/mol.119.116731
This article has not been copyedited and formatted. The final version may differ from this version.

bilaterally into the oviducts of CD-1 pseudo-pregnant females. Approximately 20-21 days following implantation, the CD-1 females gave birth. Pups were weaned 21 days after birth, ear-tagged, and tail biopsies collected. Pups were genotyped via next generation sequencing (NGS) to identify founder mice. Results confirmed two mutant strains carrying a high percentage of alleles with frame-shift causing deletions (-65 bp: 98.0%, -107 bp: 99.9%; Fig. 1B). These mice were backcrossed 3-4 generations to WT C57BL/6NCrl mice and subsequent generations were genotyped via next generation sequencing (NGS) to confirm mutations and subsequently RT-PCR (Fig. 1C). $Mct6^{-/-}$ and $Mct6^{+/+}$ mice were littermates in all experiments performed in this study.

Genotyping of $Mct6^{-/-}$ mice.

Briefly, during weaning, tail biopsies were collected and DNA was isolated using the REDExtract-N-Amp™ Tissue PCR Kit (Sigma Aldrich, St. Louis, MO), according to manufacturer's protocol. For this protocol, primers were designed to flank exon 2 of murine *Slc16a5* (Slc16a5.ex2.F (5'-3'): ATCTCTTAAGCCCCCGGCTA, Slc16a5.ex2.R: ATAAGCAGTTCCACCCACCC). The RT-PCR reactions were carried out using a BioRad CFX Connect™ RT System and *Taq* DNA Polymerase (Thermo Fisher Scientific). Cycling conditions were chosen based on the suggested manufacturer's protocol. Each reaction was heated at 94°C for 3 min, and 30 cycles were then performed as follows: denaturing at 94°C for 45 s, annealing at 60°C for 30 s, extension at 72°C for 1 min. A final extension was performed by heating at 72°C for 10 min. PCR products were then separated on a 3% agarose gel and imaged using a ChemiDoc XRS+ System (Bio-Rad, Hercules, CA).

qRT-PCR and mRNA expression in $Mct6^{-/-}$ and $Mct6^{+/+}$ mice.

In order to validate the knockout of $Mct6^{-/-}$ and to investigate mRNA expression of WT $Mct6^{+/+}$ mouse tissues, major organs (i.e. kidney, liver, lungs, brain, colon, ileum, jejunum, and duodenum) were harvested from both groups of male mice at 28-30 weeks of age (N = 3-5). Duodenum was collected as the 5 cm of the small intestine following the pylorus, and the jejunum and ileum were segmented from the residual

Molecular Pharmacology Fast Forward. Published on July 10, 2019 as DOI: 10.1124/mol.119.116731
This article has not been copyedited and formatted. The final version may differ from this version.

small intestinal tissue (two fifths and three fifths, respectively). Colon was collected as 5 cm of large intestine following the cecum. Tissues were homogenized using a VWR Pellet Mixer and total RNA was isolated and purified using an RNeasy Mini Kit (QIAGEN, Germantown, MD) according to the manufacturer's protocol. RNA concentration, purity, and stability was confirmed via a NanoDrop 1000 and FlashGel™ System. First-strand cDNA synthesis was performed using SuperScript™ III RT (Thermo Fisher Scientific) according to the manufacturer's protocol. Concentration and purity was further confirmed. For the qRT-PCR analysis, Taqman® gene expression assays were used for *Slc16a5* (Thermo Fisher Scientific, Assay ID: Mm01252138) and the housekeeping genes *Gapdh* (Assay ID: Mm99999915) and *Hprt* (Assay ID: Mm03024075). The *Slc16a5* probes spanned exons 2 and 3 of murine *Slc16a5*. All probes were labeled with FAM dye for fluorescent detection. Cycle threshold (C_t) were obtained from BioRad CFX Manager 3.0 software and imported into Excel for analysis.

Blood panel analysis and tissue weights.

Blood samples were collected via the submandibular vein from $Mct6^{+/+}$ and $Mct6^{-/-}$ male mice (N = 4, 18-19 weeks old) in heparinized tubes following an overnight fast with free access to water. Whole blood was analyzed using Prep Profile II reagent rotors via a Vetscan VS2 (Abaxis, Union City, CA) according to manufacturer's instructions. ALT, ALP, GLU, TP, and BUN were determined in $Mct6^{+/+}$ and $Mct6^{-/-}$ mice and compared to evaluate overall health and investigate physiological differences. In addition, major tissues (i.e. brain, liver, kidneys, small intestine, and colon) were harvested from $Mct6^{+/+}$ and $Mct6^{-/-}$ male mice sacrificed at 30 weeks of age (N = 10) and weighed.

Protein preparation and digestion.

Kidney, liver, and colon were isolated from $Mct6^{+/+}$ and $Mct6^{-/-}$ male mice (N = 5-6, 27-33 weeks of age-matched male mice fed normal chow and free access to water) and stored at -80°C until extraction after snap-freezing in liquid nitrogen. The protein preparation and digestion was performed as done previously (Ma et al., 2017). Briefly, the whole tissues were ground in liquid nitrogen into a fine powder, and

Molecular Pharmacology Fast Forward. Published on July 10, 2019 as DOI: 10.1124/mol.119.116731
This article has not been copyedited and formatted. The final version may differ from this version.

homogenized in ice-cold lysis buffer (50 mM Tris-formic acid (FA), 150 mM NaCl, 0.5% sodium deoxycholate, 2% sodium dodecyl sulfate (SDS), 2% NP-40, pH 8.0) with protease inhibitor tablets (Roche Applied Science, Indianapolis, IN), and were sonicated until clear. Each lysate was centrifuged at 20,000 g for 30 min at 4 °C, and the supernatant was collected. Total protein concentration was measured using a bicinchoninic acid assay (BCA) kit (Pierce Biotechnology, Inc., Rockford, IL). One hundred micrograms of extracted proteins from each sample were utilized for LC-MS/MS analysis. Reduction and alkylation of proteins were achieved by 30 min incubation with 3 mM tris (2-caboxyl) phosphine (TCEP) and 30 min incubation with 20 mM iodoacetamide (IAM). After reduction and alkylation, the surfactant-aided/on-pellet digestion (SOD) method (An et al., 2015) was employed to remove detergents and perform tryptic digestion of proteins.

Long gradient nano-reverse-phase liquid chromatography/mass spectrometry.

An UltiMate 3000 RSLCnano system and an Orbitrap Fusion Lumos mass spectrophotometer (Thermo Fisher Scientific, San Jose, CA) were used. The mobile phase A contained 2% acetonitrile in 0.1% formic acid and mobile phase B contained 88% acetonitrile in 0.1% formic acid. Four microliters of digested mixtures were loaded onto a large-ID trap (300 µm ID x 0.5 cm, packed with Zorbax 3-µm C18 material) with 1% mobile B at a flow rate of 10 µL/min for 3 min. The trapped peptides were then back-flushed onto the nano-LC column (75 µm ID x 60 cm, packed with Waters XSelect CSH 2.5 µm C18 material) at a flow rate of 250 nL/min. The nano-LC column was heated at 52°C. A 180 min gradient was used and the optimized gradient profile was as follows: 4% B over 3 min; 4 to 11% B over 5 min; 11 to 28% B over 117 min; 28 to 50% B over 10 min; 50 to 97% B over 1 min and isocratic for 17 min; and finally isocratic at 4% B for 27 min. Mass spectrometry (MS) was performed in positive ion mode and MS data were generated under data-dependent product ion scan mode with a cycle time of 3 s. A survey scan (m/z 400-1500) at a resolution of 120,000 with an AGC target of 5×10^5 and a maximum injection time of 50 ms was applied. MS2 was acquired by isolation at 1.2 Th with the quadrupole for high-energy collision dissociation fragmentation and detected by Orbitrap at a resolution of 15,000 with an AGC target of 5×10^4. The

Molecular Pharmacology Fast Forward. Published on July 10, 2019 as DOI: 10.1124/mol.119.116731
This article has not been copyedited and formatted. The final version may differ from this version.

maximum injection time of 50 ms and the normalized activation energy of 30% with a 5% of stepped collision energy were used. The activation q was 0.25. Dynamic exclusion was enabled with repeat count of one and exclusion duration of 45 s. Biological replicates from each group were analyzed in a random manner.

Protein identification and ion-current-based quantification.

The MS raw files were searched against the UniProt-Swissprot *mus musculus* protein database (released on September 2017) with a total of 16,900 protein entries using the Proteome Discoverer v1.4 (Thermo Fisher Scientific). Ten ppm tolerance for precursor ion mass, 0.02 Da for fragment ion mass with fully tryptic peptides restraint, and a maximum of two missed cleavages were allowed. Static carbamidomethylation of cysteine and dynamic oxidation of methionine were applied. The false discovery rate (FDR) was detected by using a target-decoy search strategy. Scaffold 4.5 (Proteome Software, Portland, OR) was used to validate MS/MS-based peptide and protein identification. The false discovery rates of 0.1% at peptide level and 1% at protein level were used. An ion current-based quantification method (IonStar processing pipeline) was described previously (Shen et al., 2018; Wang et al., 2018). Maximum retention time shift for alignment step was 0.2 min. The quantitative frames were determined based on m/z (width: 10 ppm) and retention time (width: 2.5 min). Peptides or frames shared among different protein groups were excluded from quantitative analysis. The ion current intensities of each protein were normalized by the LOESS method (Dunn et al., 2011). Intensities for peptides of the same protein were combined to be the protein intensity with Grubbs' test (a minimum dataset presence 2 and *p*-value cutoff of 0.01). The relative expression ratio was calculated by the average ion-current intensities of six replicates in each group. Student's t-test was used to evaluate statistical significance between groups. A $p < 0.05$ and a minimum of 1.3-fold change were used to determine the significantly altered proteins.

Liver RNA extraction, RNA-seq library preparation, and sequencing.

Molecular Pharmacology Fast Forward. Published on July 10, 2019 as DOI: 10.1124/mol.119.116731
This article has not been copyedited and formatted. The final version may differ from this version.

Total and small RNAs were isolated using the RNeasy Mini Kit (QIAGEN). Briefly, 50 mg of frozen tissue (N = 3 male mice/group) were first disrupted with a liquid nitrogen-cooled mortar and pestle. After disruption, the tissues were immediately homogenized with the addition of 700 µl of QIAzol Lysis Reagent (QIAGEN). Further homogenization was accomplished by centrifuging homogenates with a QIAshredder column (QIAGEN). After addition of chloroform, the homogenates were then separated into aqueous and organic phases by centrifugation. The upper, aqueous phases were extracted, and ethanol was added to provide appropriate binding conditions for all RNA molecules from 18 nucleotides upwards. The samples were then applied to the RNeasy Mini spin column. On-column DNAse digestion was also performed to remove any residual genomic DNA contamination followed by additional washes. High quality RNA samples were eluted in 60 µl of RNase-free water. Quantitative assessment of the purified total RNA was accomplished by using a Qubit Broad Range RNA kit (Thermo Fisher). The RNA samples were further evaluated qualitatively by a 2100 Bioanalyzer (Agilent technologies).

The sequencing libraries were prepared with the mRNA HyperPrep kit (KAPA BIOSYSTEMS), from 500 ng total RNA according to manufacturer's instructions. Fragmented RNA was reverse-transcribed into first strand cDNA using random primers. Pure Beads (KAPA BIOSYSTEMS) were used to separate the ds cDNA from the second strand reaction mix resulting in blunt-ended cDNA. A single 'A' nucleotide was then added to the 3' ends of the blunt fragments. Multiple indexing adapters, containing a single 'T' nucleotide on the 3' end of the adapter, were ligated to the ends of the ds cDNA, preparing them for hybridization onto a flow cell. Adapter ligated libraries were amplified by PCR, purified using Pure Beads, and validated for appropriate size on a 4200 TapeStation D1000 Screentape (Agilent Technologies, Inc.). The DNA libraries were quantified using KAPA Biosystems qPCR kit, and were pooled together in an equimolar fashion following experimental design criteria. Each DNA pool was denatured and diluted to 2.4 pM 1% PhiX control library. The resulting pools were then loaded into the appropriate NextSeq Reagent cartridge for 75 cycle paired-end sequencing and sequenced on a NextSeq500 following the manufacturer's recommended protocol (Illumina Inc.).

Molecular Pharmacology Fast Forward. Published on July 10, 2019 as DOI: 10.1124/mol.119.116731
This article has not been copyedited and formatted. The final version may differ from this version.

***RNA-seq analysis*.**

Raw reads that passed the quality filter from Illumina Real-Time Analysis were pre-processed by using FASTQC (v0.10.1) for sequencing base quality control. The reads were mapped to the latest murine reference genome and ENSEMBL annotation database using Tophat (v2.0.13) (Trapnell et al., 2009). A second round of QC, using RSeQC (Wang et al., 2012), was applied to mapped BAM files to identify potential RNASeq library preparation problems. From the mapping results, the read counts for genes were obtained by HTSeq (Anders et al., 2015) using the intersection-strict option. Sample relationships were explored by sample clustering, PCA, and tSNE. Differentially expressed genes were identified using DESeq2 (Love et al., 2014), a variance-analysis package developed to infer the statically significant differences in RNA-seq data. A $p < 0.05$ and a minimum of 1.5-fold change were used to determine the significantly altered genes.

Bioinformatics and pathway analysis.

DAVID was used for characterization of biological pathway and functional annotations for the 'omics data (https://david.ncifcrf.gov/) (Huang et al., 2009a; Huang et al., 2009b). Investigation into canonical pathways and network interactions were performed in Ingenuity® Pathway Analysis (IPA®, QIAGEN, Redwood City, CA, https://www.qiagenbioinformatics.com/ipa). Additional pathway analysis for the transcriptomic data was performed by Gene Set Enrichment Analysis (GSEA) using rank based gene lists from the differential expression analysis.

***Triglyceride assay*.**

Total plasma triglycerides were measured in (TG) *ad libitum* fed age-matched $Mct6^{+/+}$ and $Mct6^{-/-}$ male mice (N = 8/group, 30 weeks old) using a Triglyceride Colorimetric Assay Kit (Cayman Chemical, Ann Arbor, MI) according to manufacturer's instructions. Blood was collected from the submandibular vein into heparinized tubes on the same day and stored at -80°C until analysis.

Molecular Pharmacology Fast Forward. Published on July 10, 2019 as DOI: 10.1124/mol.119.116731
This article has not been copyedited and formatted. The final version may differ from this version.

Statistical analysis.

For mRNA expression, data was analyzed in Microsoft Excel using the $2^{-\Delta\Delta Ct}$ method (Livak and Schmittgen, 2001). For the $Mct6^{+/+}$ and $Mct6^{-/-}$ mRNA comparison, data was normalized to mRNA expression in $Mct6^{+/+}$ mice and expressed as fold change for each tissue. For mRNA tissue comparison amongst $Mct6^{+/+}$ mice, data was normalized to kidney tissue and expressed as fold change. All other statistical analyses were performed using the one-way unpaired analysis of variance (ANOVA) followed by Tukey's post hoc test to test for multiple comparisons or an unpaired Student's t-test. Differences were considered statistically significant when $p < 0.05$. For pathway analysis, a modified Fisher's Exact Test was used to verify significance of enrichment. Z scores were used as a statistical measure of the match between an expected relationship direction (i.e. activation or inhibition) and the observed differential expression ($-2 \geq Z$ is considered to be significantly inhibited and $Z \geq 2$ is considered to be significantly activated).

Molecular Pharmacology Fast Forward. Published on July 10, 2019 as DOI: 10.1124/mol.119.116731
This article has not been copyedited and formatted. The final version may differ from this version.

RESULTS

Comparative gene expression of Mct6 in Mct6$^{-/-}$ and Mct6$^{+/+}$ mice.

In order to verify the relative absence of *Mct6* gene expression in our knockout mouse model as well as characterize the relative tissue-specific gene expression in WT Mct6$^{+/+}$ mice, qRT-PCR analyses were performed using a TaqMan gene expression assay. Fig. 2A shows greater than 90% knockdown of *Mct6* (*Slc16a5*) gene expression in all major tissues analyzed when normalized to WT (Mct6$^{+/+}$) mice. No gene expression was detected in the lungs, brain, or duodenum. The greatest gene expression relative to other tissues was observed in the colon, compared to the kidney and liver, in WT mice (Fig. 2B) using two different housekeeping genes (glyceraldehyde 3-phosphate dehydrogenase (*Gapdh*) and hypoxanthine guanine phosphoribosyl transferase (*Hprt*)). This result is consistent with previously reported gene expression in C57BL/6 mice (Expression Atlas).

Phenotypic characterization of Mct6$^{-/-}$mice.

Following the generation of the Mct6$^{-/-}$ mouse model, a blood panel analysis of biomarkers for liver and kidney function, as well as overall health was performed. he Mct6$^{+/+}$ and Mct6$^{-/-}$ mice do not demonstrate any significant differences in common blood panel biomarkers including alanine aminotransferase (ALT), alkaline phosphatase (ALP), glucose (GLU), total protein (TP), and urea nitrogen (BUN) when measured at 18-19 weeks of age (data not shown). Over a period of 3-30 weeks of age, the two groups of mice did not demonstrate any significant differences in body weight.

At an age of 30 weeks of age, mice were sacrificed from the two groups and major organs were collected and weighed to investigate if there were any organ size differences between the two strains. There were no statistical differences between the two groups, and in addition, no aberrant tissue morphologies were seen upon visual examination during necropsy (data not shown). Due to these findings, Mct6$^{-/-}$ mice appeared to be healthy, with growth, physiological development and biochemistry similar to the Mct6$^{+/+}$ mice.

Proteomic profiling of organs in Mct6$^{-/-}$ and Mct6$^{+/+}$ mice.

Molecular Pharmacology Fast Forward. Published on July 10, 2019 as DOI: 10.1124/mol.119.116731
This article has not been copyedited and formatted. The final version may differ from this version.

Multi-tissue proteome profiling in Mct6$^{-/-}$ and Mct6$^{+/+}$ mice was performed with good precision and utilizing a stringent set of criteria. As shown in Fig. 3, a summary of the scheme depicts the overall paradigm of this method from sample collection and preparation to functional annotation. Using this exhaustive sample preparation and treatment procedure, over 4,000 unique proteins were identified for each tissue, which comprised of a mixture of proteins derived from multiple subcellular compartments. A stringent set of significance criteria was used to test for differences between Mct6$^{+/+}$ and Mct6$^{-/-}$ mice ($\geq$ 1.3-fold change, $p < 0.05$). A summary is provided in Fig. 4. For kidney, 4,417 unique proteins were identified with 31 significantly upregulated and 20 downregulated. For the liver, 4,124 unique proteins were identified with 16 significantly upregulated and 22 downregulated. For the colon, 4,483 unique proteins were detected with 82 significantly upregulated and 159 downregulated. Using highly stringent false discovery rates (0.1% at peptide level and 1% at protein level) and strict criteria for peptide discovery (minimum of 2 peptides and a *p*-value cutoff of 0.01), the comparative proteomic profiles between the two groups of mice are characterized with good confidence. Tables 1-3 depict the most significantly altered proteins in kidney, liver, and colon tissues respectively.

Bioinformatics and pathway characterization of proteins.

Gene ontology (GO) analysis of biological processes and molecular functions was performed for the significantly altered proteins in kidney, liver, and colon tissues using the Database for Annotation, Visualization and Integrated Discovery (DAVID) v6.8 bioinformatics tool. For all three tissues, the majority of proteins were involved in a wide range of metabolic pathways significantly altered in the Mct6$^{-/-}$ mice compared to the Mct6$^{+/+}$ mice ($p < 0.05$). Considering metabolism was the most abundant and relevant biological pathway associated with the significantly altered proteins in each tissue, all metabolic biological pathways were compared across all tissues. For tissues such as kidney and colon, GO biological pathway analysis revealed that a majority of the proteins significantly altered between the Mct6$^{+/+}$ and Mct6$^{-/-}$ mice were associated with metabolic processes (66.7%, $p = 0.047$ and 60.8%, $p = 0.038$, respectively for kidney and colon). While this GO term was not significant in the liver (possibly due to minimal significant

Molecular Pharmacology Fast Forward. Published on July 10, 2019 as DOI: 10.1124/mol.119.116731
This article has not been copyedited and formatted. The final version may differ from this version.

differences in protein expressions in this tissue), the most significantly altered GO biological pathway for this sample, as well as the most abundant, was cellular lipid metabolic processes (15.8%, $p = 0.027$). With regards to cellular localization, across all three organs, GO analysis revealed that the most significant and abundant localization of the altered proteins were in membrane-bounded organelles (kidney: 88.2%, $p = 3.5 \times 10^{-6}$; liver: 76.3%, $p = 4.4 \times 10^{-3}$; colon: 80.0%, $p = 1.8 \times 10^{-14}$).

Proteomic canonical pathway analysis and network association in organs.

Using the Ingenuity Knowledge Base in Ingenuity Pathway Analysis (IPA), the top five canonical pathways were identified using our significantly altered protein datasets for each tissue (Table 4). Pathway information was gathered through Ingenuity Target Explorer (https://targetexplorer.ingenuity.com). For the kidney, the top five pathways identified were majorly involved in immunomodulatory effects such as NF-kappaB activation, as well regulation of immune response via a variety of signaling networks. For the liver, the most significant pathway was involved in cell-to-cell adhesion; however, a variety of metabolic pathways were also significantly associated with our dataset. Interestingly, α-tocopherol degradation, a process involved in metabolizing plant-based vitamin E antioxidants via breakdown pathways such as dehydrogenation and β-oxidation pathways, was the second most significant pathway associated with our hepatic proteomic dataset. Glucose, lipid, and sterol metabolic and biosynthetic pathways were also significantly associated with our differential expression data.

Of the three tissues analyzed in this study, the colon appeared to exhibit the most significantly changed proteins in the $Mct6^{-/-}$ mice compared the $Mct6^{+/+}$ mice (colon: 241 > kidney: 51 > liver: 38). This is an interesting finding considering that intestinal tissue has been one of the primary tissues studied for MCT isoform expression due to their importance in drug absorption and fatty acid transport (Gill et al., 2005; Iwanaga et al., 2006; Kirat et al., 2006a; Kirat and Kato, 2006; Kirat et al., 2006b); Kirat et al. (2007); (Kirat and Miyasho, 2015; Kohyama et al., 2013; Welter and Claus, 2008). In addition, it is important to note that in our study the colon had the greatest WT gene expression relative to the other tissues analyzed. The most significant canonical pathway associated with our differential colon proteomic dataset was

Molecular Pharmacology Fast Forward. Published on July 10, 2019 as DOI: 10.1124/mol.119.116731
This article has not been copyedited and formatted. The final version may differ from this version.

clathrin-mediated endocytosis signaling (p = 7.49 x 10^{-4}), a prominent pathway in the intestine for the absorption of nutrients, hormones and a wide variety of other signaling molecules from the extracellular space. Interestingly, triacylglycerol biosynthesis was also significantly associated with the colon proteomic dataset (p = 1.61 x 10^{-2}), a major pathway involved in the regulation of hormone and lipid homeostasis, as well as energy metabolism.

Hepatic transcriptomic profiling in Mct6$^{-/-}$ and Mct6$^{+/+}$ mice.

Genes were considered significantly differentially expressed between the two groups of mice if there was a ≥ 1.5-fold change and $p < 0.05$. A total of 14,117 genes were detected in this assay, with 109 genes significantly upregulated and 90 genes significantly downregulated (a total of 199 significant differentially expressed genes; Supplemental Figures 1 and 2 show the top 50 up and downregulated genes, respectively. For all six samples, there were 46-50 million mapped reads, which accounted for 94-96% of the input reads. A summary of the percentage of tags assigned to main genomic features is given in Fig. 5A. Fig. 5B shows the top 15 up- and downregulated significant genes in the Mct6$^{-/-}$ mice compared to Mct6$^{+/+}$ mice, the most differentially expressed being *Slc16a5* encoding for Mct6 (log2 fold-change: -6.96, p = 2.37 x 10^{-10}). Of the top 15 downregulated genes by abundance, the top three most significant genes were *Tnfsf8* (log2 fold-change: -4.60, p = 0.0113), *Acod1* (log2 fold-change: -2.21, p = 2.90 x 10^{-3}), *Marco* (log2 fold-change: -1.76, p = 1.67 x 10^{-3}). *Tnfsf8* encodes for the CD30 ligand in immune cells, and may regulate, and be regulated by lipid levels in atherosclerosis (Foks et al., 2012; Getz and Reardon, 2014). Also, *Acod1* encodes for aconitate decarboxylase 1 and generates itaconate, a compound shown to play a role in antimicrobial activity of immune cells and indirect moderation of the TCA cycle (Luan and Medzhitov, 2016). Lastly, *Marco* encodes for a macrophage scavenger receptor that has been shown to be induced in nonalcoholic steatohepatitis (NASH) suggesting its role in high-fat diet induced hepatic pathogenesis (Yoshimatsu et al., 2004). The downregulation of these genes suggest that Mct6$^{-/-}$ may exhibit some immunosuppressive effects.

Molecular Pharmacology Fast Forward. Published on July 10, 2019 as DOI: 10.1124/mol.119.116731
This article has not been copyedited and formatted. The final version may differ from this version.

The most upregulated gene was *Acta1* (log2 fold-change: 3.75, $p = 0.0487$), a gene that encodes alpha actin a key determinant of cellular contraction. However, there was large variability surrounding this gene among samples. The most significant upregulated gene, in our top 15 upregulated dataset by abundance, was *Nr4a3* (log2 fold-change: 2.56, $p = 1.51 \times 10^{-6}$) (Fig. 5B), that encodes for nuclear receptor 4a3. Increased expression of *Nr4a3* is correlated with glucose utilization, and *Nr4a3* is important in metabolic pathways, and in different dieting states (Safe et al., 2016). The second most significantly upregulated gene was *Atf3* (log2 fold-change: 1.86, $p = 1.11 \times 10^{-5}$), encoding for a member of the ATF/cAMP-responsive element-binding protein family of transcription factors. When *Atf3* is stress-induced in the liver, it can cause defects in glucose homeostasis by downregulating gluconeogenesis (Allen-Jennings et al., 2002). The third most significantly (by *p*-value) downregulated gene in the top 15: *Slc15a2* (log2 fold-change: 1.65, $p = 2.18 \times 10^{-4}$), encodes for Pept2, a proton-dependent peptide transporter most commonly known for its importance in kidney amino acid availability (Rubio-Aliaga et al., 2003). The relevance of downregulation of this transporter in $Mct6^{-/-}$ mouse phenotypes is unknown.

Bioinformatics and pathway characterization of genes in liver.

GO analysis of biological processes and molecular functions were characterized for the significantly altered differential gene dataset in livers of $Mct6^{+/+}$ and $Mct6^{-/-}$ mice. Similar to the proteomic datasets, DAVID was used to perform a GO analysis of all biological processes and functions involved in the liver differential transcriptomic dataset. As with the other analyses, a large number of genes that were significantly differentially expressed between the two groups were associated with a variety of metabolic pathways between the two groups of mice. As in the liver proteomic data, the most significantly altered GO biological pathway for this tissue was lipid metabolic processes (22.1%, $p = 2.84 \times 10^{-10}$). With regards to cellular localization, across all three tissues, GO analysis revealed that the most significant localization of the proteins encoded for by the differentially expressed genes were in peroxisomes (5.2%, $p = 3.3 \times 10^{-4}$). Considering peroxisomes are a major site of fatty acid β-oxidation and lipid metabolism, this result was not surprising based on our previous results exhibiting changes in lipid metabolism biological pathways.

Molecular Pharmacology Fast Forward. Published on July 10, 2019 as DOI: 10.1124/mol.119.116731
This article has not been copyedited and formatted. The final version may differ from this version.

Transcriptomic canonical pathway analysis and network association in liver.

Similar to the proteomic data analyses, IPA was used to identify the top five canonical pathways using the significantly differentially expressed genes in the liver (Table 5). The top five pathways identified were primarily involved in cholesterol biosynthesis, such as the superpathway of cholesterol biosynthesis, as well as upstream regulatory pathways involved in cholesterol, terpene/terpenoid, and sterol synthesis. In addition, the majority of the pathways identified were predicted to be upregulated in our analysis. Interestingly, the mevalonate pathway I was both one of the top five canonical pathways in the proteomic dataset, as well as the transcriptomic dataset. As in the proteomic data, the canonical pathways involved in sterol metabolic and biosynthetic pathways were also shown in our transcriptomic analysis. However, due to the richer transcriptomic dataset compared to our liver proteomic dataset, we were able to predict whether these pathways were significantly activated or inhibited.

Additionally, using IPA, the principal network generated using the differential dataset was Lipid Metabolism, Small Molecule Biochemistry, Vitamin and Mineral Metabolism (Fig. 6). It is evident from the network that there is a wide range of interconnected genes involved in the regulation of lipid metabolism. In particular, *Pparα* (peroxisome proliferator-activated receptor alpha) is a key transcriptional regulator in this network, and contributes to a majority of the mechanisms involved in hepatic lipid homeostasis.

Triglyceride assay in Mct6$^{+/+}$ and Mct6$^{-/-}$ mice.

Due to preliminary evidence of Mct6's role in lipid metabolism, plasma triglycerides (TGs) were compared between the two groups of mice fed *ad libitum* to investigate if there were significant differences in overall TG exposure. Mct6$^{-/-}$ mice revealed a significant increase (p = 0.017) in plasma triglycerides (80.2 mg/dL) in comparison to the Mct6$^{+/+}$ mice (46.8 mg/dL), which represents a 1.7-fold overall increase in plasma TGs (Fig. 7).

Molecular Pharmacology Fast Forward. Published on July 10, 2019 as DOI: 10.1124/mol.119.116731
This article has not been copyedited and formatted. The final version may differ from this version.

DISCUSSION

This study represents the first *in vivo* evidence of the endogenous function of Mct6, obtained through the utilization of multi-tissue liquid chromatography/mass spectrometry (LC/MS) comparative proteomic analyses and liver transcriptomics in a novel CRISPR/Cas9 Mct6 knockout mouse model.

Development and characterization of the Mct6$^{-/-}$ mouse model.

To further investigate and characterize the functional role of MCT6 *in vivo*, our laboratory developed the first Mct6$^{-/-}$ mouse model with the utilization of CRISPR/Cas9 (Ran et al., 2013). We suspect that the residual < 10% *Slc16a5* gene expression seen in our mRNA data is due to truncated and functionally inactive mRNA variants only containing exons 3 and 4. The WT gene expression data from this study largely agrees with what is reported via Expression Atlas (G5E8K6) for *Slc16a5* expression in mice. The measures of liver/kidney function suggest that Mct6 deficiency does not impact the overall health using the biomarkers tested for in this study.

Interestingly, the increase in plasma TG exposure in Mct6$^{-/-}$ mice suggests that Mct6 may have some regulatory role in lipid metabolism. These include the possible roles of Mct6 in the elimination of TGs, or inhibition of its synthesis via direct or indirect mechanisms, which could result in higher TG concentrations in Mct6 knockout mice. Future studies are needed in order to elucidate a plausible mechanism surrounding its involvement in TG homeostasis.

Comparative proteomics and transcriptomics of Mct6$^{+/+}$ and Mct6$^{-/-}$ mice.

The majority of the significantly altered proteins were downregulated in the Mct6$^{-/-}$ mice in the colon and liver, but upregulated in the kidney. The lack of significant up/down-regulation of other Mct isoforms in these three tissues also suggests that Mct6 plays a unique role in a biological pathway that is not significantly compensated for by other Mcts. Interestingly, the number of significantly altered proteins in each tissue also correlates well with the relative gene expression of Mct6 in that tissue. From the RNA-seq analysis, it was expected that the most downregulated gene in our Mct6$^{-/-}$ mice was *Slc16a5*, which further

Molecular Pharmacology Fast Forward. Published on July 10, 2019 as DOI: 10.1124/mol.119.116731
This article has not been copyedited and formatted. The final version may differ from this version.

validated the inactivation of *Mct6* gene expression. Many of the most significantly altered genes in the Mct6$^{-/-}$ mice, by magnitude and *p*-value, were shown to be involved in regulating lipid and glucose levels, as well as lipid signaling pathways. This finding supports the previous hypothesis by Zhang et al. which proposed that *Slc16a5* may play a role in pathways such as glucose and lipid metabolism (Zhang et al., 2011b).

In addition, a drawback to the analyses performed in this study is the incomplete validation of the proteomic and transcriptomic data using additional assays. Our lab initially investigated Mct6 protein expression through commercially available antibodies, however this was unsuccessful mostly due to reasons involving the presence of multiple bands and lack of reliability of antibody-based detection methods. Attempts are currently ongoing to assess the metabolic and regulatory consequences that Mct6$^{-/-}$ mice have on glucose/lipid metabolism, and to determine as to whether or not the magnitude of these changes play a meaningful impact on downstream biomarkers. However, recently Xu et al. has provided evidence for MCT6's role in glucose and lipid metabolism using a rat model for diabetes (Xu et al., 2019). The study demonstrated that intestinal MCT6 function and expression was impaired in diabetic rats induced by combination of high-fat diet and low dose of streptozocin. Though this study was performed in rats, it provides a supporting example that MCT6 plays a major role in these pathways and warrants further investigation.

Bioinformatics analysis on kidney proteomic data.

Investigation into the significantly differentially expressed proteins in the kidney of Mct6$^{-/-}$ mice revealed a wide range of metabolic processes, including lipid metabolism and network functions associated with cellular function and maintenance. IPA revealed that the top canonical pathways associated with the kidney dataset were immunomodulatory pathways. Considering that changes in the lipid metabolism have been demonstrated to play a role in modulating the immune system (de Pablo and Alvarez de Cienfuegos, 2000; Wu et al., 2018), perturbation in the renal secretion or reabsorption of dietary fatty acids via deactivation of Mct6 may be responsible for affecting these immunomodulatory events. One such group of

Molecular Pharmacology Fast Forward. Published on July 10, 2019 as DOI: 10.1124/mol.119.116731
This article has not been copyedited and formatted. The final version may differ from this version.

immunomodulatory signaling molecules are the prostaglandins, large chain fatty acids of the eicosanoid family synthesized from dietary fat, and responsible for a wide range of biochemical events including regulation of the immune system (Harris et al., 2002; Ricciotti and FitzGerald, 2011). Moreover, considering there is evidence that prostaglandin $F_{2\alpha}$ is a substrate for MCT6 (Murakami et al., 2005), this transporter may play a role in regulating the immune system through this pathway: however, further mechanistic studies are needed to confirm this hypothesis.

Bioinformatics analysis on liver proteomic data.

The top three significant GO biological pathways from our liver proteomic data were cellular lipid metabolism, mitochondrion organization, and fatty acid metabolism; these findings are supported with transcriptomic data suggesting that Mct6 is involved in lipid metabolism (Zhang et al., 2011b). In addition, IPA bioinformatics analysis revealed that the top associated network functions included energy production and lipid metabolism. As previously mentioned, one of the top canonical pathways included α-tocopherol degradation, which involves the breakdown of plant-based vitamin E antioxidants responsible for terminating free-radical induced lipid peroxidation (Singal et al., 2011; van Acker et al., 2000).

Additionally, glycogen biosynthesis from UDP-D-glucose also surfaced as a significant canonical pathway associated with our altered protein dataset. Like lipids, glycogen is a major storage form of energy, strictly regulated by hormones and nutritional status (Lu et al., 2014). The crosstalk of lipogenesis and glycogenesis is largely responsible for moderating energy storage and regulating ATP production. Additional significantly altered metabolic pathways include the mevalonate pathway and pregnenolone biosynthesis, both representing precursors necessary for steroid hormone biosynthesis and regulatory pathways in lipid homeostasis. Overall, it is evident from our limited dataset for the liver, that there are significant alterations in the hepatic proteome of $Mct6^{-/-}$ mice, associated with diet-associated lipid, and potentially glucose metabolism, which agree with previous transcriptomic reports (Lu et al., 2011; Zhang et al., 2011b).

Molecular Pharmacology Fast Forward. Published on July 10, 2019 as DOI: 10.1124/mol.119.116731
This article has not been copyedited and formatted. The final version may differ from this version.

Bioinformatics analysis on colon proteomic data.

Bioinformatics analysis performed on the differential colon proteomic data from the $Mct6^{+/+}$ and $Mct6^{-/-}$ mice (which was the most abundant in all three tissues analyzed: 241 significantly altered proteins), was consistent with the kidney and liver data, which revealed the pathways containing the most abundant proteins were largely metabolic. The clathrin-mediated endocytosis-signaling pathway, which was characterized as the most significant pathway in our colon dataset, is largely responsible for the absorption of a wide range of dietary molecules. In particular, it has also been implicated as a major process of lipid raft-mediated absorption of low-density lipoproteins, which include triglycerides, lipids, and cholesterol. This process if tightly regulated via lipid composition and microdomain organization of the plasma membrane, which is highly dependent on a variety of functional lipid metabolic pathways (Harayama and Riezman, 2018).

Additionally, a large number of proteins involved in the TG biosynthesis pathway were differentially expressed between the two groups of mice. Changes in this pathway in the $Mct6^{-/-}$ mice would most likely cause changes in tissue or systemic TG concentrations, depending on the magnitude of change. This hypothesis is supported by our finding of significantly altered plasma TG concentrations. In intestinal tissue, TGs are synthesized and packaged in order to supply nutrients to peripheral tissues that can impact a wide variety of metabolic pathways (Yen et al., 2015). Perturbation of this pathway can have a direct effect on regulation of hormones, as well as lipid metabolism and overall systemic energy balance.

Bioinformatics analysis on liver transcriptomic data.

The most significant pathway enriched and predicted to be activated was the superpathway of cholesterol biosynthesis, which included upregulation of *Pmvk, Sqle, Idi1, Fdps, Hmgcr, Cyp51a1,* and *Mvd*. Specifically, *Hmgcr* encodes for the protein HMG-CoA reductase, a rate-limiting step in cholesterol biosynthesis, which has been shown to be activated in the liver during a high fat diet (Wu et al., 2013). The mevalonate pathway overlaps the activity of this enzyme, by which mevalonate is synthesized from HMG-CoA to generate isoprenoids, including cholesterol, steroid hormones, and other lipid molecules.

Molecular Pharmacology Fast Forward. Published on July 10, 2019 as DOI: 10.1124/mol.119.116731
This article has not been copyedited and formatted. The final version may differ from this version.

This pathway analysis is supported by the large number of significant genes associated with lipid metabolism that are altered in our analysis. The genome-wide association study in the Genetics of Lipid Lowering Drugs and Diet Network (GOLDN; n=872) identified a variant (rs12949451) in a predicted enhancer/promoter region of *SLC16A5* in humans that was associated with triglyceride response to a high fat meal (Wojczynski et al., 2015). Further mechanistic studies are needed to verify the impact of this variant on *SLC16A5* activity and its relation to lipid metabolism.

Conclusions and future directions.

For the first time using a multi-omics approach and a novel knockout mouse model, our investigation revealed evidence that MCT6 may play a role in glucose/lipid metabolism. However, further investigations are needed to assess potential changes following different diets, such as high fat diets, which may reveal significant differences in glucose and lipid metabolic markers. These data, along with additional validation experiments such as a comprehensive metabolomic analysis, will provide additional support for these potential changes seen in these pathways. Further exploration is needed to provide evidence for a specific role of Mct6 within these pathways, and for the investigation of MCT6 as a potential therapeutic target in disease.

Molecular Pharmacology Fast Forward. Published on July 10, 2019 as DOI: 10.1124/mol.119.116731
This article has not been copyedited and formatted. The final version may differ from this version.

ACKNOWLEDGEMENTS

We would also like to acknowledge Mark D. Parker for his assistance in the mouse colony breeding scheme and guidance throughout the course of the study.

Molecular Pharmacology Fast Forward. Published on July 10, 2019 as DOI: 10.1124/mol.119.116731
This article has not been copyedited and formatted. The final version may differ from this version.

AUTHOR CONTRIBUTIONS

Participated in research design: Jones and Morris

Conducted experiments: Jones, Tu, Zheng, and Qu

Contributed new analytical tools: Jones, Tu, Zheng, and Qu

Performed data analysis: Jones, Tu, Zheng and Morris

Contributed to writing of the manuscript: Jones, Tu, and Morris

Molecular Pharmacology Fast Forward. Published on July 10, 2019 as DOI: 10.1124/mol.119.116731
This article has not been copyedited and formatted. The final version may differ from this version.

REFERENCES

Abe S, Namba N, Abe M, Fujiwara M, Aikawa T, Kogo M and Ozono K (2012) Monocarboxylate transporter 10 functions as a thyroid hormone transporter in chondrocytes. *Endocrinology* **153**(8): 4049-4058.

Allen-Jennings AE, Hartman MG, Kociba GJ and Hai T (2002) The roles of ATF3 in liver dysfunction and the regulation of phosphoenolpyruvate carboxykinase gene expression. *The Journal of biological chemistry* **277**(22): 20020-20025.

An B, Zhang M, Johnson RW and Qu J (2015) Surfactant-aided precipitation/on-pellet-digestion (SOD) procedure provides robust and rapid sample preparation for reproducible, accurate and sensitive LC/MS quantification of therapeutic protein in plasma and tissues. *Analytical chemistry* **87**(7): 4023-4029.

Anders S, Pyl PT and Huber W (2015) HTSeq--a Python framework to work with high-throughput sequencing data. *Bioinformatics* **31**(2): 166-169.

Castorino JJ, Gallagher-Colombo SM, Levin AV, FitzGerald PG, Polishook J, Kloeckener-Gruissem B, Ostertag E and Philp NJ (2011) Juvenile Cataract-Associated Mutation of Solute Carrier SLC16A12 Impairs Trafficking of the Protein to the Plasma Membrane. *Invest Ophth Vis Sci* **52**(9): 6774-6784.

de Pablo MA and Alvarez de Cienfuegos G (2000) Modulatory effects of dietary lipids on immune system functions. *Immunology and cell biology* **78**(1): 31-39.

Dhayat N, Simonin A, Anderegg M, Pathare G, Luscher BP, Deisl C, Albano G, Mordasini D, Hediger MA, Surbek DV, Vogt B, Sass JO, Kloeckener-Gruissem B and Fuster DG (2016) Mutation in the Monocarboxylate Transporter 12 Gene Affects Guanidinoacetate Excretion but Does Not Cause Glucosuria. *J Am Soc Nephrol* **27**(5): 1426-1436.

Dumitrescu AM, Liao XH, Weiss RE, Millen K and Refetoff S (2006) Tissue-specific thyroid hormone deprivation and excess in monocarboxylate transporter (mct) 8-deficient mice. *Endocrinology* **147**(9): 4036-4043.

Dunn WB, Broadhurst D, Begley P, Zelena E, Francis-McIntyre S, Anderson N, Brown M, Knowles JD, Halsall A, Haselden JN, Nicholls AW, Wilson ID, Kell DB, Goodacre R and Human Serum Metabolome C (2011) Procedures for large-scale metabolic profiling of serum and plasma using gas chromatography and liquid chromatography coupled to mass spectrometry. *Nat Protoc* **6**(7): 1060-1083.

Foks AC, Bot I, Frodermann V, de Jager SC, Ter Borg M, van Santbrink PJ, Yagita H, Kuiper J and van Puijvelde GH (2012) Interference of the CD30-CD30L pathway reduces atherosclerosis development. *Arteriosclerosis, thrombosis, and vascular biology* **32**(12): 2862-2868.

Friesema EC, Ganguly S, Abdalla A, Manning Fox JE, Halestrap AP and Visser TJ (2003) Identification of monocarboxylate transporter 8 as a specific thyroid hormone transporter. *J Biol Chem* **278**(41): 40128-40135.

Getz GS and Reardon CA (2014) The mutual interplay of lipid metabolism and the cells of the immune system in relation to atherosclerosis. *Clinical lipidology* **9**(6): 657-671.

Gill RK, Saksena S, Alrefai WA, Sarwar Z, Goldstein JL, Carroll RE, Ramaswamy K and Dudeja PK (2005) Expression and membrane localization of MCT isoforms along the length of the human intestine. *American journal of physiology Cell physiology* **289**(4): C846-852.

Halestrap AP and Meredith D (2004) The SLC16 gene family - from monocarboxylate transporters (MCTs) to aromatic amino acid transporters and beyond. *Pflug Arch Eur J Phy* **447**(5): 619-628.

Harayama T and Riezman H (2018) Understanding the diversity of membrane lipid composition. *Nature reviews Molecular cell biology*.

Harris SG, Padilla J, Koumas L, Ray D and Phipps RP (2002) Prostaglandins as modulators of immunity. *Trends Immunol* **23**(3): 144-150.

Huang DW, Sherman BT and Lempicki RA (2009a) Bioinformatics enrichment tools: paths toward the comprehensive functional analysis of large gene lists. *Nucleic Acids Res* **37**(1): 1-13.

Huang DW, Sherman BT and Lempicki RA (2009b) Systematic and integrative analysis of large gene lists using DAVID bioinformatics resources. *Nat Protoc* **4**(1): 44-57.

Iwanaga T, Takebe K, Kato I, Karaki S and Kuwahara A (2006) Cellular expression of monocarboxylate transporters (MCT) in the digestive tract of the mouse, rat, and humans, with special reference to slc5a8. *Biomedical research* **27**(5): 243-254.

Jones RS and Morris ME (2016) Monocarboxylate Transporters: Therapeutic Targets and Prognostic Factors in Disease. *Clinical pharmacology and therapeutics* **100**(5): 454-463.

Jones RS, Parker MD and Morris ME (2017) Quercetin, Morin, Luteolin, and Phloretin Are Dietary Flavonoid Inhibitors of Monocarboxylate Transporter 6. *Molecular pharmaceutics*.

Kirat D, Inoue H, Iwano H, Hirayama K, Yokota H, Taniyama H and Kato S (2006a) Monocarboxylate transporter 1 gene expression in the ovine gastrointestinal tract. *Veterinary journal* **171**(3): 462-467.

Kirat D and Kato S (2006) Monocarboxylate transporter 1 (MCT1) mediates transport of short-chain fatty acids in bovine caecum. *Experimental physiology* **91**(5): 835-844.

Kirat D, Masuoka J, Hayashi H, Iwano H, Yokota H, Taniyama H and Kato S (2006b) Monocarboxylate transporter 1 (MCT1) plays a direct role in short-chain fatty acids absorption in caprine rumen. *The Journal of physiology* **576**(Pt 2): 635-647.

Kirat D, Matsuda Y, Yamashiki N, Hayashi H and Kato S (2007) Expression, cellular localization, and functional role of monocarboxylate transporter 4 (MCT4) in the gastrointestinal tract of ruminants. *Gene* **391**(1-2): 140-149.

Kirat D and Miyasho T (2015) Regional and cellular distribution of monocarboxylate transporters 13 and 14 in the cattle gastrointestinal tract. *Cell Mol Biol* **61**(3): 39-45.

Kohyama N, Shiokawa H, Ohbayashi M, Kobayashi Y and Yamamoto T (2013) Characterization of Monocarboxylate Transporter 6: Expression in Human Intestine and Transport of the Antidiabetic Drug Nateglinide. *Drug Metab Dispos* **41**(11): 1883-1887.

Livak KJ and Schmittgen TD (2001) Analysis of relative gene expression data using real-time quantitative PCR and the 2(-Delta Delta C(T)) Method. *Methods* **25**(4): 402-408.

Love MI, Huber W and Anders S (2014) Moderated estimation of fold change and dispersion for RNA-seq data with DESeq2. *Genome Biol* **15**(12): 550.

Lu BB, Bridges D, Yang YM, Fisher K, Cheng AA, Chang L, Meng ZX, Lin JD, Downes M, Yu RT, Liddle C, Evans RM and Saltiel AR (2014) Metabolic Crosstalk: Molecular Links Between Glycogen and Lipid Metabolism in Obesity. *Diabetes* **63**(9): 2935-2948.

Lu Y, Boekschoten MV, Wopereis S, Muller M and Kersten S (2011) Comparative transcriptomic and metabolomic analysis of fenofibrate and fish oil treatments in mice. *Physiol Genomics* **43**(23): 1307-1318.

Luan HH and Medzhitov R (2016) Food Fight: Role of Itaconate and Other Metabolites in Antimicrobial Defense. *Cell metabolism* **24**(3): 379-387.

Ma JH, Shen S, Wang JJ, He Z, Poon A, Li J, Qu J and Zhang SX (2017) Comparative Proteomic Analysis of the Mitochondria-associated ER Membrane (MAM) in a Long-term Type 2 Diabetic Rodent Model. *Scientific reports* **7**(1): 2062.

Murakami Y, Kohyama N, Kobayashi Y, Ohbayashi M, Ohtani H, Sawada Y and Yamamoto T (2005) Functional characterization of human monocarboxylate transporter 6 (SLC16A5). *Drug Metab Dispos* **33**(12): 1845-1851.

Ran FA, Hsu PD, Wright J, Agarwala V, Scott DA and Zhang F (2013) Genome engineering using the CRISPR-Cas9 system. *Nat Protoc* **8**(11): 2281-2308.

Ricciotti E and FitzGerald GA (2011) Prostaglandins and inflammation. *Arteriosclerosis, thrombosis, and vascular biology* **31**(5): 986-1000.

Rubio-Aliaga I, Frey I, Boll M, Groneberg DA, Eichinger HM, Balling R and Daniel H (2003) Targeted disruption of the peptide transporter Pept2 gene in mice defines its physiological role in the kidney. *Molecular and cellular biology* **23**(9): 3247-3252.

Rusu V, Hoch E, Mercader JM, Tenen DE, Gymrek M, Hartigan CR, DeRan M, von Grotthuss M, Fontanillas P, Spooner A, Guzman G, Deik AA, Pierce KA, Dennis C, Clish CB, Carr SA, Wagner BK, Schenone M, Ng MCY, Chen BH, Consortium M, Consortium STD, Centeno-Cruz F,

Zerrweck C, Orozco L, Altshuler DM, Schreiber SL, Florez JC, Jacobs SBR and Lander ES (2017) Type 2 Diabetes Variants Disrupt Function of SLC16A11 through Two Distinct Mechanisms. *Cell* **170**(1): 199-212 e120.

Safe S, Jin UH, Morpurgo B, Abudayyeh A, Singh M and Tjalkens RB (2016) Nuclear receptor 4A (NR4A) family - orphans no more. *The Journal of steroid biochemistry and molecular biology* **157**: 48-60.

Schwartz CE, May MM, Carpenter NJ, Rogers RC, Martin J, Bialer MG, Ward J, Sanabria J, Marsa S, Lewis JA, Echeverri R, Lubs HA, Voeller K, Simensen RJ and Stevenson RE (2005) Allan-Herndon-Dudley syndrome and the monocarboxylate transporter 8 (MCT8) gene. *Am J Hum Genet* **77**(1): 41-53.

Shen X, Shen S, Li J, Hu Q, Nie L, Tu C, Wang X, Poulsen DJ, Orsburn BC, Wang J and Qu J (2018) IonStar enables high-precision, low-missing-data proteomics quantification in large biological cohorts. *Proceedings of the National Academy of Sciences of the United States of America*.

Singal AK, Jampana SC and Weinman SA (2011) Antioxidants as therapeutic agents for liver disease. *Liver International* **31**(10): 1432-1448.

Trapnell C, Pachter L and Salzberg SL (2009) TopHat: discovering splice junctions with RNA-Seq. *Bioinformatics* **25**(9): 1105-1111.

van Acker FAA, Schouten O, Haenen GRMM, van der Vijgh WJF and Bast A (2000) Flavonoids can replace alpha-tocopherol as an antioxidant. *FEBS letters* **473**(2): 145-148.

Wang L, Wang S and Li W (2012) RSeQC: quality control of RNA-seq experiments. *Bioinformatics* **28**(16): 2184-2185.

Wang X, Niu J, Li J, Shen X, Shen S, Straubinger RM and Qu J (2018) Temporal Effects of Combined Birinapant and Paclitaxel on Pancreatic Cancer Cells Investigated via Large-Scale, Ion-Current-Based Quantitative Proteomics (IonStar). *Molecular & cellular proteomics : MCP* **17**(4): 655-671.

Welter H and Claus R (2008) Expression of the monocarboxylate transporter 1 (MCT1) in cells of the porcine intestine. *Cell biology international* **32**(6): 638-645.

Wojczynski MK, Parnell LD, Pollin TI, Lai CQ, Feitosa MF, O'Connell JR, Frazier-Wood AC, Gibson Q, Aslibekyan S, Ryan KA, Province MA, Tiwari HK, Ordovas JM, Shuldiner AR, Arnett DK and Borecki IB (2015) Genome-wide association study of triglyceride response to a high-fat meal among participants of the NHLBI Genetics of Lipid Lowering Drugs and Diet Network (GOLDN). *Metabolism: clinical and experimental* **64**(10): 1359-1371.

Wu N, Sarna LK, Hwang SY, Zhu Q, Wang P, Siow YL and O K (2013) Activation of 3-hydroxy-3-methylglutaryl coenzyme A (HMG-CoA) reductase during high fat diet feeding. *Biochimica et biophysica acta* **1832**(10): 1560-1568.

Wu W, Shi X and Xu C (2018) Regulation of T cell signalling by membrane lipids. *Nature reviews Immunology* **18**(3): 219.

Xu F, Zhu L, Qian C, Zhou J, Geng D, Li P, Xuan W, Wu F, Zhao K, Kong W, Qin Y, Liang L, Liu L and Liu X (2019) Impairment of Intestinal Monocarboxylate Transporter 6 Function and Expression in Diabetic Rats Induced by Combination of High-Fat Diet and Low Dose of Streptozocin: Involvement of Butyrate-Peroxisome Proliferator-Activated Receptor-gamma Activation. *Drug metabolism and disposition: the biological fate of chemicals* **47**(6): 556-566.

Yen CL, Nelson DW and Yen MI (2015) Intestinal triacylglycerol synthesis in fat absorption and systemic energy metabolism. *Journal of lipid research* **56**(3): 489-501.

Yoshimatsu M, Terasaki Y, Sakashita N, Kiyota E, Sato H, van der Laan LJ and Takeya M (2004) Induction of macrophage scavenger receptor MARCO in nonalcoholic steatohepatitis indicates possible involvement of endotoxin in its pathogenic process. *International journal of experimental pathology* **85**(6): 335-343.

Zhang F, Xu X, Zhou B, He Z and Zhai Q (2011a) Gene expression profile change and associated physiological and pathological effects in mouse liver induced by fasting and refeeding. *PloS one* **6**(11): e27553.

Zhang F, Xu X, Zhou B, He Z and Zhai Q (2011b) Gene expression profile change and associated physiological and pathological effects in mouse liver induced by fasting and refeeding. *PloS one* **6**(11): e27553.

Molecular Pharmacology Fast Forward. Published on July 10, 2019 as DOI: 10.1124/mol.119.116731
This article has not been copyedited and formatted. The final version may differ from this version.

FOOTNOTES

Funding support was from the National Institutes of Health National Institute on Drug Abuse [Grant R01DA023223] and an IMPACT grant from the University at Buffalo. RSJ was supported in part by a PhRMA Pre- Doctoral Graduate Fellowship.

Molecular Pharmacology Fast Forward. Published on July 10, 2019 as DOI: 10.1124/mol.119.116731
This article has not been copyedited and formatted. The final version may differ from this version.

FIGURE LEGENDS

Figure 1. Generation of Mct6$^{-/-}$ mice. Exon 2 was targeted in the *Slc16a5* gene (A) using CRISPR/Cas9 technology with two short guide RNAs (gRNA1 and gRNA2). NGS of the founder pups confirmed two mutant strains carrying a high percentage of alleles with out-of-frame mutations (-65 bp: 98.0%, -107 bp: 99.9%; gRNA sites shown underlined in green and mutations in red) (B). 3% agarose gel electrophoresis of RT-PCR products of founder progeny demonstrating the presence of two different mutations (-65 bp, -107 bp) (C) (HOM: Mct6$^{-/-}$, HET: Mct6$^{+/-}$, WT: Mct6$^{+/+}$).

Figure 2. mRNA expression of *Slc16a5* (Mct6). All gene expression data were normalized to a housekeeping gene (*Gapdh* or *Hprt*). Data were plotted as mean fold change (F.C.) ± S.E.M (N = 3-5 male mice, 30 weeks of age). N.D.: not detected. (A) Mct6$^{-/-}$ *Slc16a5* expression normalized to Mct6$^{+/+}$ *Slc16a5* expression in each tissue. (B) *Slc16a5* expression in Mct6$^{+/+}$ mice normalized to kidney tissue (**$p < 0.01$, ***$p < 0.001$, ANOVA with Tukey's test for multiple comparisons compared to kidney and liver tissues).

Figure 3. Comparative proteomics scheme used for the kidney, liver, and colon tissue analyses in Mct6$^{+/+}$ and Mct6$^{-/-}$ male mice. An exhaustive ion current-based LC/MS/MS quantification was utilized for each tissue for each group (N = 5-6 biological replicates). DAVID and IPA were utilized as *in silico* tools to functionally annotate the significant proteins (figure adapted from Ma et al. (Ma et al., 2017)).

Figure 4. A summary of the significantly altered proteins in Mct6$^{-/-}$ male mice compared to Mct6$^{+/+}$ male mice (≥ 1.3-fold change, $p < 0.05$).

Figure 5. (A) Percentage of reads and tag distribution for each genomic feature for each sample (Mct6$^{+/+}$ and Mct6$^{-/-}$ biological replicates (1) through (3)). (B) The top 15 significantly up- (red) and downregulated (green) genes ($p < 0.05$) in Mct6$^{-/-}$ male mice compared to Mct6$^{+/+}$ male mice. The dashed lined represents the cutoff (F.C. ≥ 1.5).

Figure 6. Subcellular network depiction of the most significant putative biological process in the Mct6$^{-/-}$ male mice compared to the Mct6$^{+/+}$ male mice: Lipid Metabolism, Small Molecule Biochemistry, Vitamin and Mineral Metabolism. Genes upregulated or downregulated in Mct6$^{-/-}$ mice are represented in red or green color respectively (IL1B: interleukin-1 beta, ADRB: adrenergic receptor beta, VNN1: vanin 1,

Molecular Pharmacology Fast Forward. Published on July 10, 2019 as DOI: 10.1124/mol.119.116731
This article has not been copyedited and formatted. The final version may differ from this version.

MARCO: macrophage receptor MARCO, FDPS: farnesyl pyrophosphate synthase, CYP4A11: cytochrome P450 4A11, SQLE: squalene epoxidase, CYP51A1: cytochrome P450 4A11, HMGCR: 3-hydroxy-3-methylglutaryl-coenzyme A reductase, IDI1: isopentenyl-diphosphate delta-isomerase 1, PTK6: protein-tyrosine kinase 6, FABP2: fatty acid-binding protein 2, TXNIP: thioredoxin-interacting protein, PMVK: phosphomevalonate kinase, MVD: diphosphomevalonate decarboxylase, RETSAT: all-trans-retinol 13,14-reductase, ACOT2: acyl-coenzyme A thioesterase 2, ACACB: acetyl-CoA carboxylase 2, ACOT1: acyl-coenzyme A thioesterase 1, ALDH3A2: Fatty aldehyde dehydrogenase 3A2, ACLY: ATP-citrate synthase, ACSS2: acetyl-coenzyme A synthetase, PPARA: peroxisome proliferator-activated receptor alpha, CCNA2: cyclin-A2, Nr1h: nuclear receptor 1h, BCL3: B-cell lymphoma 3 protein homolog, FKBP5: Peptidyl-prolyl cis-trans isomerase FKBP5, FOSB: protein fosB, UBD: ubiquitin D, TOP2A: DNA topoisomerase 2-alpha, THRSP: thyroid hormone-inducible hepatic protein, ONECUT1: hepatocyte nuclear factor). Solid lines represent direct interactions and dashed lines represent indirect interactions. The network was constructed using IPA (QIAGEN).

Figure 7. Plasma TG concentrations in $Mct6^{+/+}$ and $Mct6^{-/-}$ male mice (N = 8/group, * $p = 0.017$, Student t-test). Data is presented as mean +/- S.D.

Molecular Pharmacology Fast Forward. Published on July 10, 2019 as DOI: 10.1124/mol.119.116731
This article has not been copyedited and formatted. The final version may differ from this version.

TABLES

Table 1. Top 20 significantly up- or downregulated proteins in Mct6$^{-/-}$ and Mct6$^{+/+}$ mice in kidney

Rank	Protein accession	Symbol	Protein name	Ratio (KO/WT)	p_{adj} value*
			UPREGULATED		
1	Q8K358	Pigu	Phosphatidylinositol glycan anchor biosynthesis class U	6.30	0.0073
2	P11835	Itgb2	Integrin beta-2	2.48	0.0299
3	Q64437	Adh7	Alcohol dehydrogenase class 4 mu/sigma chain	2.31	0.0422
4	F8VQB6	Myo10	Unconventional myosin-X	1.98	0.0020
5	Q8CG71	P3h2	Prolyl 3-hydroxylase 2	1.89	0.0211
6	Q7TQK1	Ints7	Integrator complex subunit 7	1.81	0.0243
7	P14483	H2-Ab1	H-2 class II histocompatibility antigen, A beta chain	1.71	0.0368
8	Q9JI99	Sgpp1	Sphingosine-1-phosphate phosphatase 1	1.69	0.0388
9	Q9DC63	Fbxo3	F-box only protein 3	1.61	0.0272
10	Q60680	Chuk	Inhibitor of nuclear factor kappa-B kinase subunit alpha	1.60	0.0458
11	Q99JR5	Tinagl1	Tubulointerstitial nephritis antigen-like	1.56	0.0427
12	Q9JK23	Psmg1	Proteasome assembly chaperone 1	1.52	0.0273
13	Q64345	Ifit3	Interferon-induced protein with tetratricopeptide repeats 3	1.50	0.0225
14	P17183	Eno2	Gamma-enolase	1.49	0.0187
15	Q9ERV1	Mkrn2	Probable E3 ubiquitin-protein ligase makorin-2	1.48	0.0158
16	O08739	Ampd3	AMP deaminase 3	1.46	0.0153
17	Q7TMV3	Fastkd5	FAST kinase domain-containing protein 5, mitochondrial	1.43	0.0224
18	Q99K41	Emilin1	EMILIN-1	1.42	0.0373
19	Q6PF93	Pik3c3	Phosphatidylinositol 3-kinase catalytic subunit type 3	1.41	0.0131
20	Q6P4S8	Ints1	Integrator complex subunit 1	1.41	0.0242
			DOWNREGULATED		
1	Q9D1C3	Pyurf	Protein preY, mitochondrial	0.06	0.0033
2	Q9D7G0	Prps1	Ribose-phosphate pyrophosphokinase 1	0.48	0.0492
3	Q8R3L5	Slco3a1	Solute carrier organic anion transporter family member 3A1	0.54	0.0051
4	Q810D6	Grwd1	Glutamate-rich WD repeat-containing protein 1	0.55	0.0475
5	Q8C0L6	Paox	Peroxisomal N(1)-acetyl-spermine/spermidine oxidase	0.60	0.0219
6	P60904	Dnajc5	DnaJ homolog subfamily C member 5	0.61	0.0082
7	Q922P9	Glyr1	Putative oxidoreductase	0.63	0.0224
8	P62482	Kcnab2	Voltage-gated potassium channel subunit beta-2	0.63	0.0163
9	Q99P87	Retn	Resistin	0.63	0.0011
10	Q80UP3	Dgkz	Diacylglycerol kinase zeta	0.63	0.0415
11	Q9CQE7	Ergic3	Endoplasmic reticulum-Golgi intermediate compartment protein 3	0.64	0.0367
12	Q7TT37	Ikbkap	Elongator complex protein 1	0.67	0.0326
13	Q9Z120	Mettl1	tRNA (guanine-N(7)-)-methyltransferase	0.68	0.0404

Molecular Pharmacology Fast Forward. Published on July 10, 2019 as DOI: 10.1124/mol.119.116731
This article has not been copyedited and formatted. The final version may differ from this version.

14	Q8R429	Atp2a1	Sarcoplasmic/endoplasmic reticulum calcium ATPase 1	0.69	0.0253
15	Q5SF07	Igf2bp2	Insulin-like growth factor 2 mRNA-binding protein 2	0.70	0.0236
16	O35226	Psmd4	26S proteasome non-ATPase regulatory subunit 4	0.71	0.0023
17	Q9Z2C5	Mtm1	Myotubularin	0.74	0.0291
18	Q6NZB0	Dnajc8	DnaJ homolog subfamily C member 8	0.75	0.0234
19	O70496	Clcn7	H(+)/Cl(-) exchange transporter 7	0.76	0.0258
20	O35609	Scamp3	Secretory carrier-associated membrane protein 3	0.77	0.0248

*p-values were calculated using a Student t-test adjusted using the Benjamini-Hochberg-FDR method.

Molecular Pharmacology Fast Forward. Published on July 10, 2019 as DOI: 10.1124/mol.119.116731
This article has not been copyedited and formatted. The final version may differ from this version.

Table 2. Top 20 significantly up- or downregulated proteins in Mct6$^{-/-}$ and Mct6$^{+/+}$ mice in liver

Rank	Protein accession	Symbol	Protein name	Ratio (KO/WT)	p_{adj} value*
			UPREGULATED		
1	Q9D4H1	Exoc2	Exocyst complex component 2	3.66	0.0095
2	Q8K2L8	Trappc12	Trafficking protein particle complex subunit 12	2.62	0.0030
3	P97426	Ear1	Eosinophil cationic protein 1	2.11	0.0420
4	Q91ZP3	Lpin1	Phosphatidate phosphatase	1.90	0.0104
5	A2AQ25	Skt	Sickle tail protein	1.89	0.0060
6	Q4VA53	Pds5b	Sister chromatid cohesion protein PDS5 homolog B	1.75	0.0420
7	Q4U2R1	Herc2	E3 ubiquitin-protein ligase	1.67	0.0247
8	Q9D0K1	Pex13	Peroxisomal membrane protein	1.67	0.0041
9	Q69Z37	Samd9l	Sterile alpha motif domain-containing protein 9-like	1.62	0.0152
10	O35943	Fxn	Frataxin, mitochondrial	1.40	0.0043
11	P16045	Lgals1	Galectin-1	1.39	0.0369
12	P68373	Tuba1c	Tubulin alpha-1C chain	1.35	0.0066
13	Q9D7X8	Ggct	Gamma-glutamylcyclotransferase	1.34	0.0165
14	Q9R062	Gyg1	Glycogenin-1	1.32	0.0336
15	Q80XI3	Eif4g3	Eukaryotic translation initiation factor 4 gamma 3	1.31	0.0464
16	Q3URF8	Kctd21	BTB/POZ domain-containing protein KCTD21	1.30	0.0459
			DOWNREGULATED		
1	Q5SX79	Shroom1	Protein Shroom1	0.50	0.0141
2	Q9QUM0	Itga2b	Integrin alpha-Iib	0.58	0.0146
3	Q9Z0H1	Wdr46	WD repeat-containing protein 46	0.62	0.0270
4	Q8BXB6	Slco2b1	Solute carrier organic anion transporter family member 2B1	0.62	0.0005
5	Q9DBA9	Gtf2h1	General transcription factor IIH subunit 1	0.63	0.0340
6	Q61136	Prpf4b	Serine/threonine-protein kinase PRP4 homolog	0.65	0.0342
7	A2CG49	Kalrn	Kalirin	0.65	0.0212
8	Q9CWN7	Cnot11	CCR4-NOT transcription complex subunit 11	0.65	0.0169
9	Q8K558	Treml1	Trem-like transcript 1 protein	0.67	0.0400
10	O88833	Cyp4a10	Cytochrome P450 4A10	0.68	0.0021
11	P62254	Ube2g1	Ubiquitin-conjugating enzyme E2 G1	0.68	0.0064
12	Q6XVG2	Cyp2c54	Cytochrome P450 2C54	0.69	0.0296
13	Q99JF5	Mvd	Diphosphomevalonate decarboxylase	0.69	0.0216
14	Q3UHJ0	Aak1	AP2-associated protein kinase 1	0.71	0.0475
15	Q8K124	Plekho2	Pleckstrin homology domain-containing family O member 2	0.72	0.0293
16	Q3UUQ7	Pgap1	GPI inositol-deacylase	0.73	0.0017
17	Q920I9	Wdr7	WD repeat-containing protein 7	0.74	0.0179
18	P58735	Slc26a1	Sulfate anion transporter 1	0.74	0.0460

Molecular Pharmacology Fast Forward. Published on July 10, 2019 as DOI: 10.1124/mol.119.116731
This article has not been copyedited and formatted. The final version may differ from this version.

19	Q91V08	Clec2d	C-type lectin domain family 2 member D	0.74	0.0282
20	Q9CQT9		Uncharacterized protein C20orf24 homolog	0.74	0.0143

*p-values were calculated using a Student t-test adjusted using the Benjamini-Hochberg-FDR method.

Molecular Pharmacology Fast Forward. Published on July 10, 2019 as DOI: 10.1124/mol.119.116731
This article has not been copyedited and formatted. The final version may differ from this version.

Table 3. Top 20 significantly up- or downregulated proteins in Mct6$^{-/-}$ and Mct6$^{+/+}$ mice in colon

Rank	Protein accession	Symbol	Protein name	Ratio (KO/WT)	p_{adj} value*
UPREGULATED					
1	P27005	S100a8	Protein S100-A8	3.22	0.0252
2	Q9D1H8	Mrpl53	39S ribosomal protein L53, mitochondrial	2.66	0.0162
3	Q80X41	Vrk1	Serine/threonine-protein kinase VRK1	2.43	0.0086
4	Q80WC3	Tnrc18	Trinucleotide repeat-containing gene 18 protein	2.25	0.0002
5	Q9JHZ2	Ankh	Progressive ankylosis protein	2.17	0.0179
6	Q7TQ62	Podn	Podocan	1.91	0.0426
7	E9PZQ0	Ryr1	Ryanodine receptor 1	1.91	0.0012
8	Q9QXE7	Tbl1x	F-box-like/WD repeat-containing protein	1.84	0.0330
9	Q8BN21	Vrk2	Serine/threonine-protein kinase	1.83	0.0314
10	Q61247	Serpinf2	Alpha-2-antiplasmin	1.83	0.0129
11	Q62432	Smad2	Mothers against decapentaplegic homolog 2	1.79	0.0408
12	Q3V384	Afg1l	AFG1-like ATPase	1.79	0.0041
13	Q9DCZ1	Gmpr	GMP reductase 1	1.79	0.0016
14	Q9CZV8	Fbxl20	F-box/LRR-repeat protein 20	1.74	0.0009
15	Q8BFQ8	Gatd1	Glutamine amidotransferase-like class 1 domain-containing protein 1	1.71	0.0067
16	Q8BFR4	Gns	N-acetylglucosamine-6-sulfatase	1.68	0.0100
17	Q3TFD2	Lpcat1	Lysophosphatidylcholine acyltransferase 1	1.67	0.0291
18	Q61555	Fbn2	Fibrillin-2	1.64	0.0384
19	Q6P5C5	Smug1	Single-strand selective monofunctional uracil DNA glycosylase	1.60	0.0028
20	P06684	C5	Complement C5	1.58	0.0221
DOWNREGULATED					
1	P02802	Mt1	Metallothionein-1	0.15	0.0096
2	P28667	Marcksl1	MARCKS-related protein	0.15	0.0022
3	Q9CQG0	Tmed6	Transmembrane emp24 domain-containing protein 6	0.21	0.0411
4	Q3TBD2	Arhgap45	Rho GTPase-activating protein 45	0.24	0.0441
5	P02798	Mt2	Metallothionein-2	0.33	0.0144
6	Q8VE97	Srsf4	Serine/arginine-rich splicing factor 4	0.39	0.0078
7	Q9WV02	Rbmx	RNA-binding motif protein, X chromosome	0.40	0.0140
8	Q5DTM8	Rnf20	E3 ubiquitin-protein ligase BRE1A	0.40	0.0025
9	P52927	Hmga2	High mobility group protein HMGI-C	0.41	0.0338
10	Q80XU3	Nucks1	Nuclear ubiquitous casein and cyclin-dependent kinase substrate 1	0.41	0.0036
11	P40240	Cd9	CD9 antigen	0.43	0.0183
12	Q71RI9	Kyat3	Kynurenine-oxoglutarate transaminase 3	0.47	0.0003
13	Q61189	Clns1a	Methylosome subunit pICln	0.47	0.0002
14	Q69Z69	Esco1	N-acetyltransferase	0.48	0.0037
15	Q8CH36	Slc36a4	Proton-coupled amino acid transporter	0.48	0.0029

Molecular Pharmacology Fast Forward. Published on July 10, 2019 as DOI: 10.1124/mol.119.116731
This article has not been copyedited and formatted. The final version may differ from this version.

16	Q7TT18	Atf7ip	Activating transcription factor 7-interacting protein 1	0.51	0.0235
17	P98078	Dab2	Disabled homolog 2	0.51	0.0013
18	Q11127	Fut4	Alpha-(1,3)-fucosyltransferase 4	0.52	0.0018
19	Q9CQ49	Ncbp2	Nuclear cap-binding protein subunit 2	0.52	0.0015
20	Q80YS6	Afap1	Actin filament-associated protein 1	0.53	0.0209

*p-values were calculated using a Student t-test adjusted using the Benjamini-Hochberg-FDR method.

Molecular Pharmacology Fast Forward. Published on July 10, 2019 as DOI: 10.1124/mol.119.116731
This article has not been copyedited and formatted. The final version may differ from this version.

Table 4. Top five canonical pathways significantly enriched with the differential protein expression data between the $Mct6^{-/-}$ and $Mct6^{+/+}$ mice.

KIDNEY	
Name	***p*-value***
NF-B Activation by Viruses	7.76×10^{-3}
Lymphotoxin Receptor Signaling	8.13×10^{-3}
Angiopoietin Signaling	1.02×10^{-2}
CD40 Signaling	2.42×10^{-2}
Role of NFAT in Regulation of the Immune Response	2.42×10^{-2}
LIVER	
Name	***p*-value**
Remodeling of Epithelial Adherens Junctions	7.76×10^{-3}
α-tocopherol Degradation	8.13×10^{-3}
Glycogen Biosynthesis II (from UDP-D-Glucose)	1.02×10^{-2}
Mevalonate Pathway I	2.42×10^{-2}
Pregnenolone Biosynthesis	2.42×10^{-2}
COLON	
Name	***p*-value**
Clathrin-mediated Endocytosis Signaling	7.49×10^{-4}
Glioma Invasiveness Signaling	1.06×10^{-2}
EIF2 Signaling	1.49×10^{-2}
Triacylglycerol Biosynthesis	1.61×10^{-2}
Regulation of Actin-based Motility by Rho	1.97×10^{-2}

**p*-values were calculated using a Fisher's Exact Test

Molecular Pharmacology Fast Forward. Published on July 10, 2019 as DOI: 10.1124/mol.119.116731
This article has not been copyedited and formatted. The final version may differ from this version.

Table 5. Top five canonical pathways significantly enhanced, based on the differential transcriptomic data between the $Mct6^{-/-}$ and $Mct6^{+/+}$ mice

Name	*p*-value*	Z-score[a]	Molecules
Superpathway of Cholesterol Biosynthesis	3.72×10^{-8}	2.65	*Pmvk, Sqle, Idi1, Fdps, Hmgcr, Cyp51a1, Mvd*
Superpathway of Geranylgeranyldiphosphate Biosynthesis I (via Mevalonate)	1.22×10^{-6}	2.24	*Pmvk, Idi1, Fdps, Hmgcr, Mvd*
Mevalonate Pathway I	9.55×10^{-6}	2	*Pmvk, Idi1, Hmgcr, Mvd*
Trans, trans-farnesyl Diphosphate Biosynthesis	5.37×10^{-4}	NaN	*Idi1, Fdps*
LPS/IL-1 Mediated Inhibition of RXR Function	8.91×10^{-4}	2	*Aldh3a2, Il1b, Cyp4a11, Cyp3a5, Pppara, Gstp1, Fabp2, Sult1c2*

**p*-values were calculated using a Fisher's Exact Test

[a]Pathways highlighted in red are predicted to be statistically significantly increased ($Z \geq 2$)

Molecular Pharmacology Fast Forward. Published on July 10, 2019 as DOI: 10.1124/mol.119.116731
This article has not been copyedited and formatted. The final version may differ from this version.

FIGURES

Figure 1

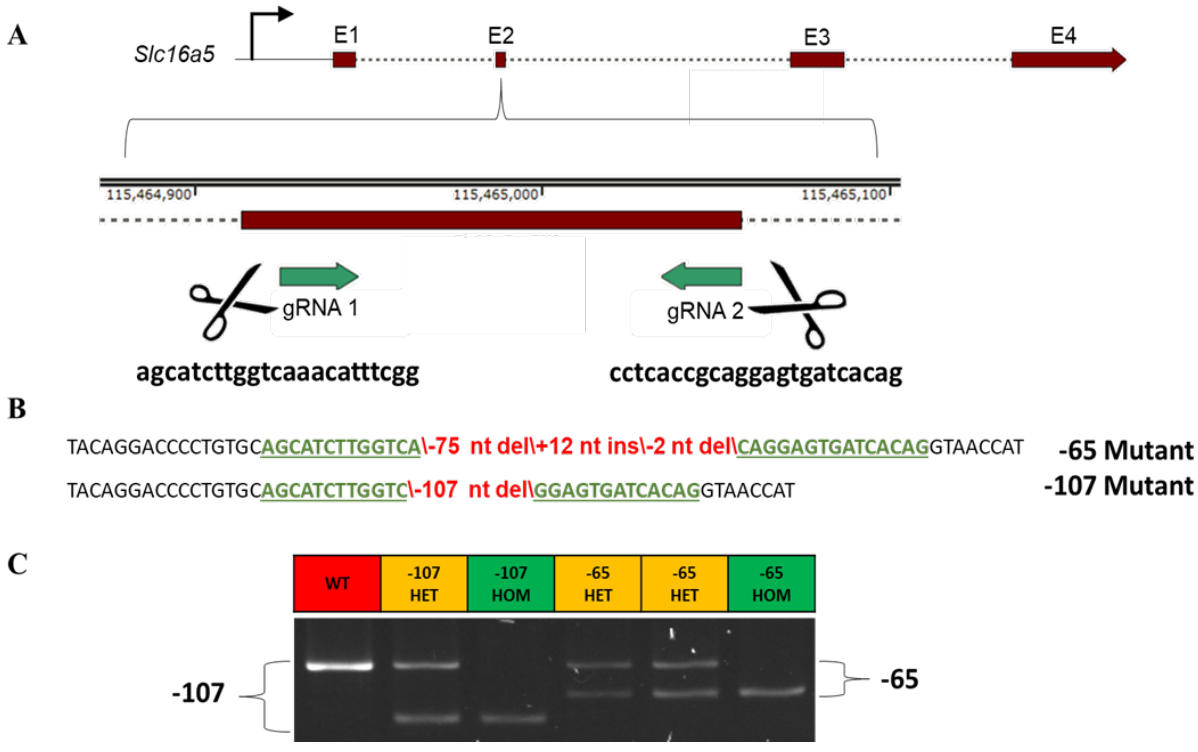

Molecular Pharmacology Fast Forward. Published on July 10, 2019 as DOI: 10.1124/mol.119.116731
This article has not been copyedited and formatted. The final version may differ from this version.

Figure 2

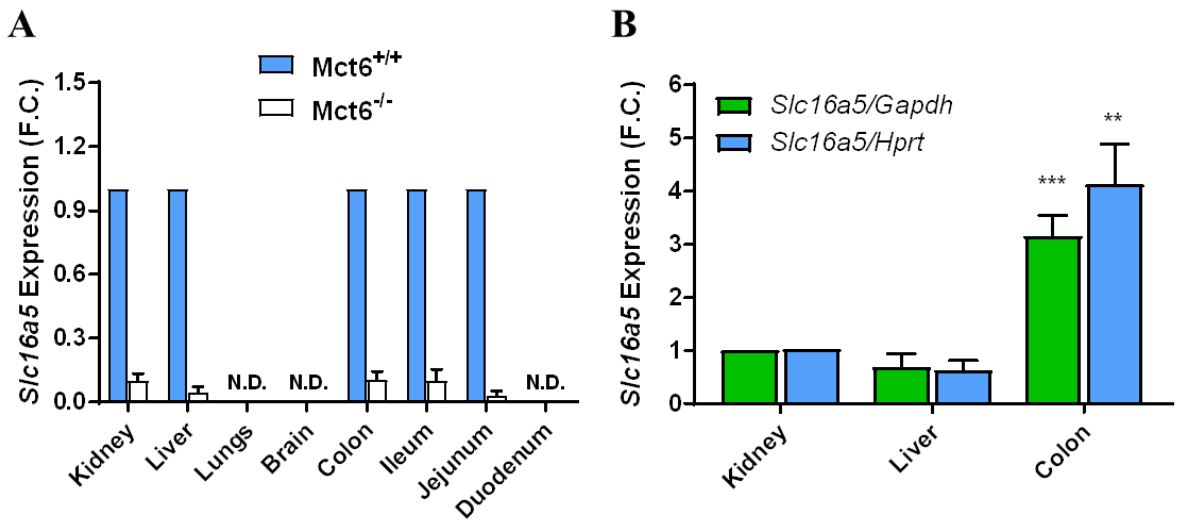

Molecular Pharmacology Fast Forward. Published on July 10, 2019 as DOI: 10.1124/mol.119.116731
This article has not been copyedited and formatted. The final version may differ from this version.

Figure 3

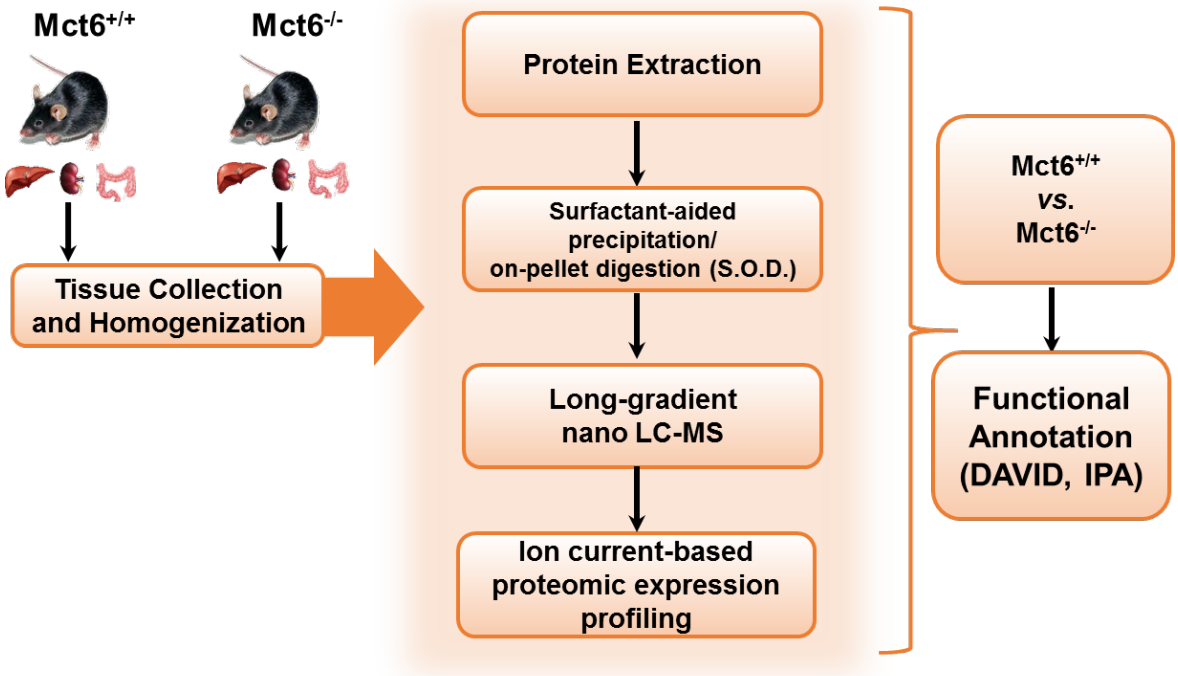

Molecular Pharmacology Fast Forward. Published on July 10, 2019 as DOI: 10.1124/mol.119.116731
This article has not been copyedited and formatted. The final version may differ from this version.

Figure 4

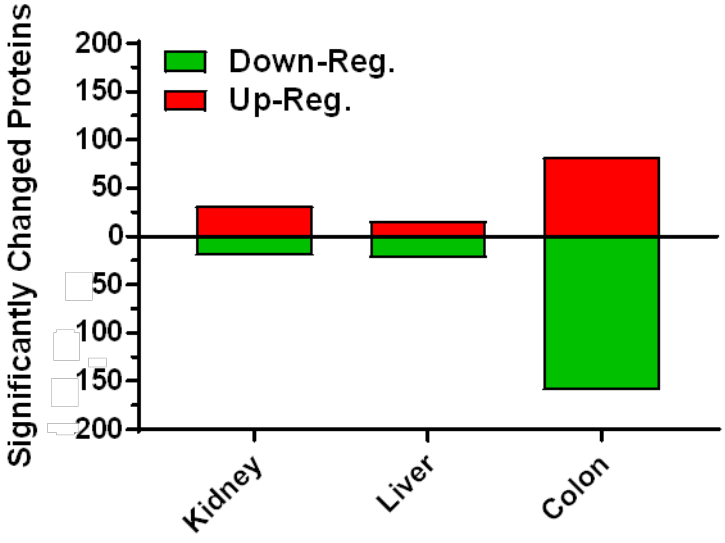

Molecular Pharmacology Fast Forward. Published on July 10, 2019 as DOI: 10.1124/mol.119.116731
This article has not been copyedited and formatted. The final version may differ from this version.

Figure 5

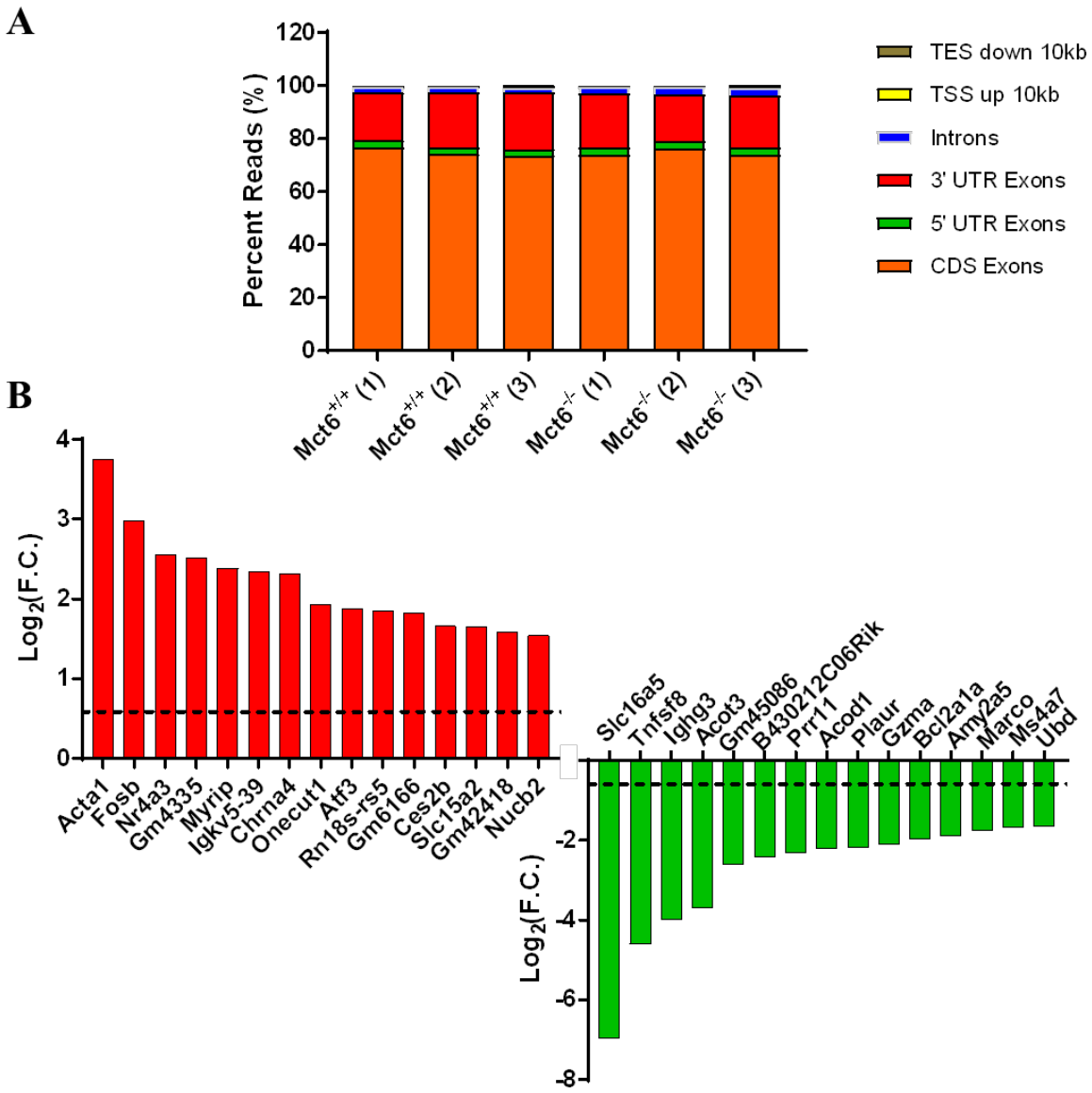

Molecular Pharmacology Fast Forward. Published on July 10, 2019 as DOI: 10.1124/mol.119.116731
This article has not been copyedited and formatted. The final version may differ from this version.

Figure 6

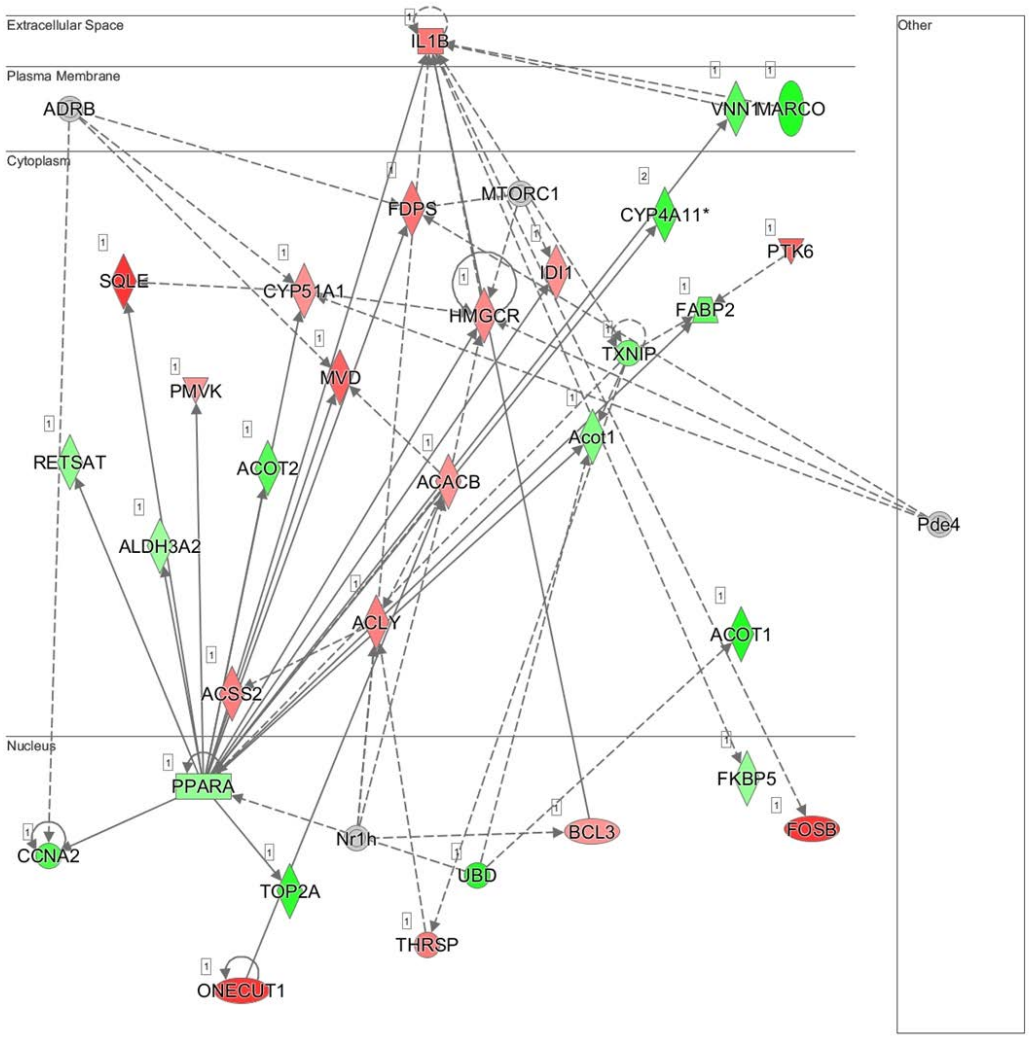

Molecular Pharmacology Fast Forward. Published on July 10, 2019 as DOI: 10.1124/mol.119.116731
This article has not been copyedited and formatted. The final version may differ from this version.

Figure 7

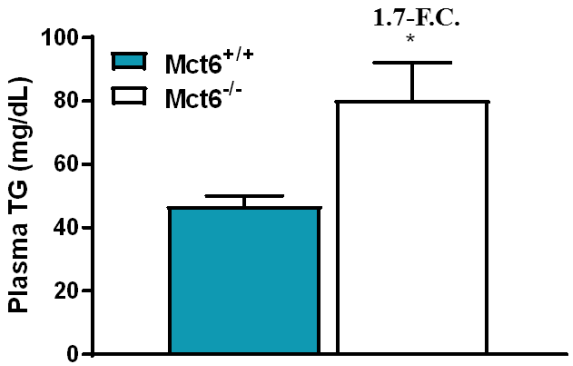

Characterization and proteomic-transcriptomic investigation of monocarboxylate transporter 6 (Mct6) knockout mice: evidence of a role in glucose and lipid metabolism

Authors: Robert S. Jones [1], Chengjian Tu [1,2], Ming Zhang [2], Jun Qu [1,2], and Marilyn E. Morris [1, *]

[1] Department of Pharmaceutical Sciences, School of Pharmacy and Pharmaceutical Sciences, University at Buffalo, State University of New York, Buffalo, New York 14214, USA

[2] New York State Center of Excellence in Bioinformatics and Life Sciences, 701 Ellicott Street, Buffalo, NY, USA

Journal: *Molecular Pharmacology*

SUPPLEMENTAL FIGURES

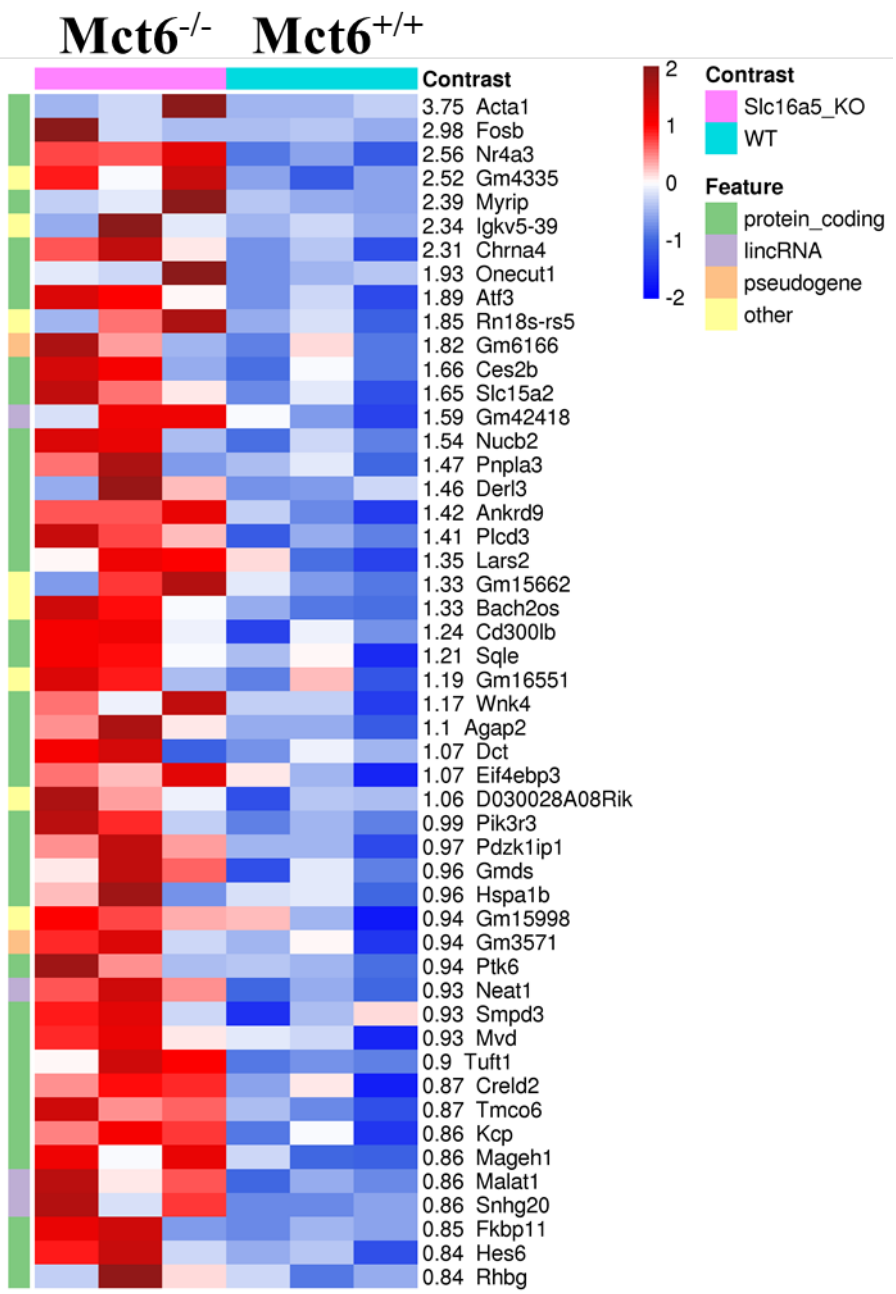

Supplemental Figure 1. Heat map showing the top 50 significantly upregulated genes expressed in Mct6$^{-/-}$ mice compared to Mct6$^{+/+}$ mice in the liver. (Slc16a5 KO: Mct6$^{-/-}$, WT: Mct6$^{+/+}$). Values represent the $\log_2$(F.C.) differential gene expression between Mct6$^{-/-}$ and Mct6$^{+/+}$ mice.

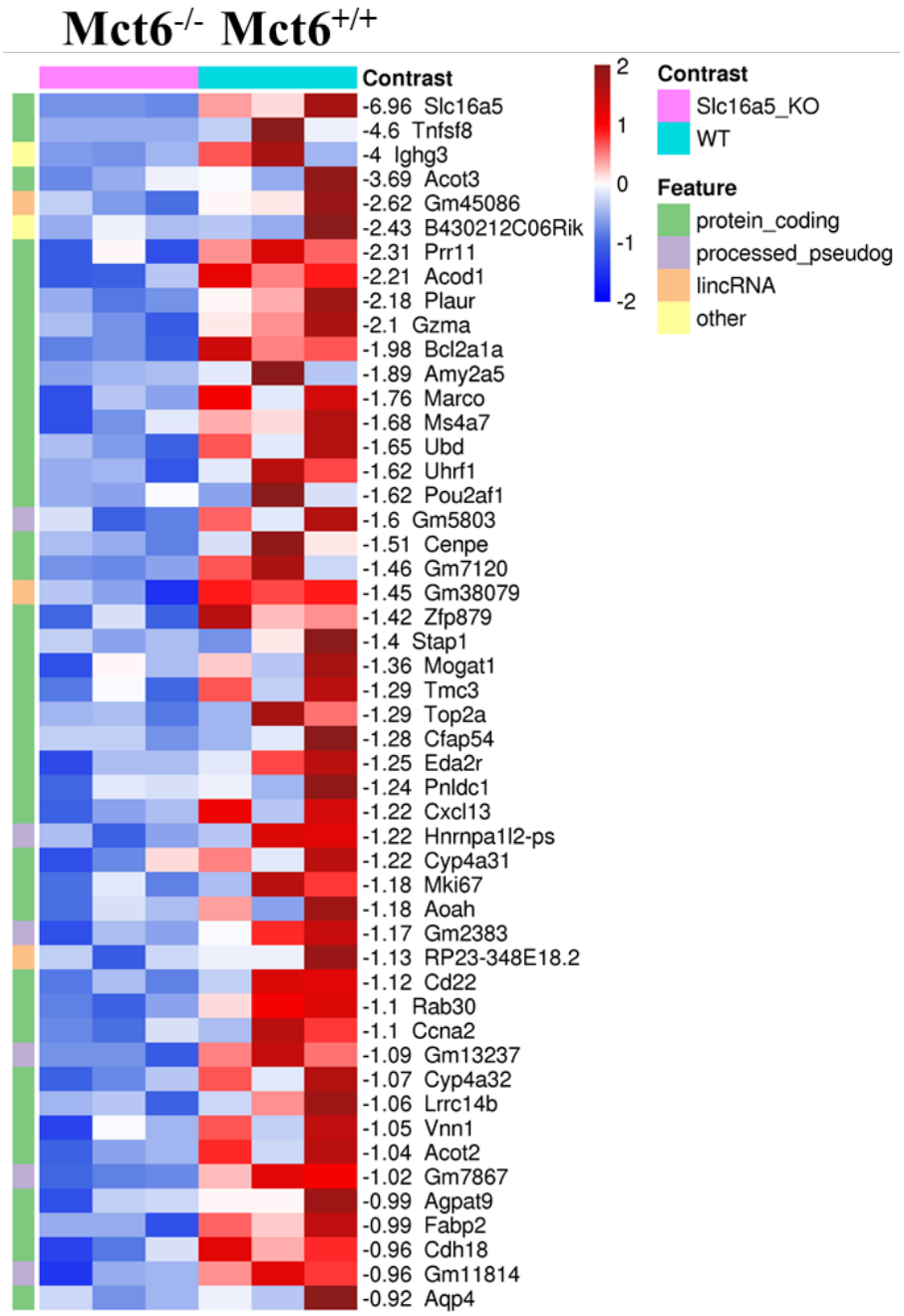

Supplemental Figure 2. Heat map showing the top 50 significantly downregulated genes expressed in Mct6$^{-/-}$ mice compared to Mct6$^{+/+}$ mice in the liver. (Slc16a5 KO: Mct6$^{-/-}$, WT: Mct6$^{+/+}$). Values represent the $\log_2$(F.C.) differential gene expression between Mct6$^{-/-}$ and Mct6$^{+/+}$ mice.